Synthesis and Characterization of Mullite Ceramics from Diphasic Aluminosilicate Gels Using Waste Driven Silica for Dielectric Application

Ermias Abebe Negash

A Thesis Submitted to

The Department of Materials Science and Engineering,

School of Mechanical, Chemical and Materials Engineering

Presented in Partial Fulfillment of the Requirement for the Degree of Master's in Materials Science and Engineering

Office of Graduate Studies

Adama Science and Technology University

June, 2024

Adama, Ethiopia

Synthesis and Characterization of Mullite Ceramics from Diphasic Aluminosilicate Gels Using Waste Driven Silica for Dielectric Application

Prepared by: Ermias Abebe Negash

ID: PGR/27954/15

Advisor: Getinet Asrat (PhD)

Co-Advisor: Belay Brehane (PhD)

A Thesis Submitted to the Department of Materials Science and Engineering,
School of Mechanical, Chemical, and Materials Engineering
Presented in Partial Fulfillment of the Requirement for the Degree of Master's
in Materials Science and Engineering
Office of Graduate Studies
Adama Science and Technology University

June, 2024

Adama, Ethiopia

Declaration

I hereby declare that this Master's Thesis entitled “Synthesis and Characterization of Mullite Ceramics from Diphasic Aluminosilicate Gels Using Waste Driven Silica for Dielectric Application” is my work and it has not been submitted for the award of any academic degree, diploma, or certificate in any other university. All the sources of materials used in this thesis have been duly acknowledged through citations.

_____	_____	_____
Name of student	Signature	Date

Recommendation of Advisor

I/We, the advisors of this thesis, hereby certify that I have closely advised/supervised the student while developing this proposal and read the draft thesis entitled "Synthesis and Characterization of Mullite Ceramics from Diphasic Aluminosilicate Gels Using Waste Driven Silica for Dielectric Application*"* prepared under my guidance by Ermias Abebe. Therefore, I/we recommend the submission of the revised version of the thesis to the department following the applicable procedures.

_____	_____	_____
Major Advisor/Supervisor	Signature	Date
_____	_____	_____
Co-advisor/Co-supervisor	Signature	Date

Approval Page

I/we, the advisors of the thesis entitled “Synthesis and Characterization of Mullite Ceramics from Diphasic Aluminosilicate Gels Using Waste Driven Silica for Dielectric Application “by Ermias Abebe hereby certify that the recommendations and suggestions made by the board of examiners are appropriately incorporated into the final version of the thesis.

_____	_____	_____
Major Advisor/Supervisor	Signature	Date

_____	_____	_____
Co-advisor/ Co-supervisor	Signature	Date

Approval of Board of Examiners

We, the undersigned, members of the Board of Examiners of the thesis by Ermias Abebe have read and evaluated the thesis entitled “Synthesis and Characterization of Mullite Ceramics from Diphasic Aluminosilicate Gels Using Waste Driven Silica for Dielectric Application” and examined the candidates during open defense. This is, therefore, to certify that the thesis is accepted for partial fulfillment of the requirement of the degree of Master of Science in material science and Engineering

Chairperson	Signature	Date
Reviewer 1	Signature	Date
Reviewer 2	Signature	Date

Finally, approval and acceptance of the thesis/dissertation proposal are contingent upon the submission of its final copy to the Office of Postgraduate Studies (OPGS) through the Department Graduate Council (DGC) and School Graduate Committee (SGC)

Department Head	Signature	Date
School Dean	Signature	Date
Office of Postgraduate Studies, Dean	Signature	

ACKNOWLEDGMENTS

First of all, I praise the Lord God Almighty for providing me with the mercy, power and grace to carry out this work. Foremost, I would like to express my deep and sincere gratitude to my research advisor, Dr. Getinet Asirat for his encouragement, and timely and constructive insightful comments and support. I would like to express my gratitude to my co-adviser Dr. Belay Brehane for his valuable advice and insightful comments. I would like to thank all the staff of material science and engineering, as well as the technical staff, especially Mr. Demeke Tesfaye, for his support. Thanks to Dr. Gebisa Bekele Head of the Materials Science and Engineering Department for his encouragement, advice and help at time of need. I am grateful to Adama Science and Technology University, especially the School of Mechanical, Chemical, and Material Science and Engineering, for their valuable support. Additionally, I thanks to Addis Ababa University for they are allow me to conduct dielectric strength test. I am extremely grateful to my parents for their love, prayers, caring, and sacrifices in educating and preparing me for my future. I would like to extend my gratitude to Mr. Yonas Asfaw from Changwon National University for his encouragement and assistance with the SEM characterization. Last but not least, I would like to thank my classmates, relatives, and friends who shared their support in one way or another. I thank Miss Ruth Mesfin, Mr. Yeabsira Sisay and Mr. Tamirat Adis for their encouragement and assistance.

Contents

LIST OF FIGURES

LIST OF TABLES

ACRONOMY

BET	Brunauer-Emmett-Teller
CVD	Chemical Vapor Deposition
DTA	Differential Thermo gravimetric Analysis
EDS	Energy-dispersive X-ray spectroscopy
FA	Fly ash
FT-IR	Fourier transform infrared
SEM	Scanning Electron Microscopy
TEOS	Tetraethyl orthosilicate
TGA	Thermo Gravimetric Analysis
XRD	X-Ray Diffraction

ABSTRACT

Our world is highly concerned about increasing energy demand and the disposal of solid wastes. For instance, the advanced ceramics industry is one of the main energy-demanding sectors and known for its expensive starting materials. Mullite ceramics are advanced ceramics and promising materials for dielectric applications and energy storage applications. Traditional methods for the formation of mullite ceramics from clay and kaolinite require above 1500^0C temperatures to become dense and form single phases. On the other hand, waste utilization as starting material result in the formation of unnecessary phases above 1450^0C and gives poor quality, but it is cost-effective and environmentally sustainable. However, sol-gel methods offer lower temperature synthesis and pure product, but are hindered by expensive precursors. In this study, mullite ceramics were synthesized using a diphasic gel process employing waste-derived silica gel as the silica precursor. The purity of the silica gel is evaluated using XRD, and FTIR characterization techniques. Based on diphasic methods mullization temperature about 1350^0C for two hours, optimal conditions for mullite synthesis were achieved with 30 ml concentration of silica gel mixed with 0.34M aluminum nitrate nonahydrate, resulting in homogeneous, stable, and pure-phase mullite. Various characterization techniques used to characterize mullite phase formations and transformation, including XRD, SEM/EDS, FTIR, and TGA/DTA. Mullite crystallization began at 1150^0C and reach single mullite phase at 1250^0C. The electrical properties of the synthesized mullite ceramics were evaluated based on temperature variations at 1150, 1250, and 1350°C for 2 hrs, and the results were about 3 kV/mm, 6.4 kV/mm, and 10.2 kV/mm, respectively. The synthesized mullite ceramics exhibited excellent electrical properties, reaching a maximum of 10.2 kV/mm. Although phase formation played a role in the performance of the mullite ceramics, the electrical properties were found to depend on the degree of densification, which led to a reduction in porosity and, thus, decreased sites for electrical breakdown. The SEM images confirmed the formation of a dense body at 1350°C for 2 h. Additionally, densification proved by the physical properties of the synthesized mullite ceramics were determined to be 0.89% water absorption, 3.02 g/cm^3 density, and 0.81% porosity, and the compression strength was found to be 420 MPa, indicating that the material is strong enough to withstand loads. Therefore, these synthesized mullite ceramics are suitable for dielectric applications.

Key words: Mullite, Diphasic, Aluminosilicate gels, Sol-gel, Silica gel, Dielectric

INTRODUCTION

1.1 Background of the Study

Mullite ($3Al_2O_3.2SiO_2$) is the only stable compound in the Al_2O_3–SiO_2 phase diagram at ambient pressures. It occurs in a narrow, temperature-dependent, solid solution range between 58 and 63 mol% Al_2O_3 (Aksay et al., 1991; Biswal et al., 2021a; Johnson et al., 2001; Lee et al., 2003; Yuvakkumar et al., 2014). This material is noteworthy because of its exceptional thermal stability, high corrosion resistance, low thermal expansion, excellent thermal shock resistance, superior creep resistance, and low thermal and electrical conductivity. Moreover, mullite ceramics exhibit impressive mechanical properties including strength and fracture toughness, making them suitable for a wide array of technical applications (Mahnicka-Goremikina et al., 2023; Xia et al., 2022). These applications include traditional products, such as porcelain, tableware, and refractories, as well as advanced materials, such as heat exchangers, filters, catalytic converters, substrates, electronic packaging devices, components for optical systems and turbine engines, and heat shields (Krenzel et al., 2019; Romero et al., 2021).

Technical mullite is synthesized through the decomposition of clays and kaolinite, which are alumino-silicate minerals. These minerals, including kyanite, andalusite, and sillimanite, are known to transform into mullite and silica upon thermal treatment (Bradt, 2008; Kim et al., 2003). This process involves mullite precursors can be prepared by adding alumina in a wet medium and firing at 1480^0C (Sánchez-Soto et al., 2018). However, because of the high impurity oxide content in natural starting materials such as Fe_2O_3, TiO_2, Na_2O, and CaO, the resulting ceramics and refractory products often contain glass phases, which can reduce their mechanical stability at high temperatures (Romero et al., 2021; Sánchez-Soto et al., 2018). This makes them less desirable for advanced ceramics and expensive in terms of energy consumption. Additionally, despite the availability of the starting material, the final product contains inclusions that can negatively affect its mechanical and electrical properties (Kim et al., 2003).

The mullite formation mechanism offers three ways to reduce the temperature based on at which the reaction starts, making it economically viable and producing a pure product. First, the use of more reactive and pure raw materials can facilitate the dissolution stage, as lower temperatures are

required for sufficient quantities of Al^{3+} ions to diffuse through the silico-aluminous liquid (Boccaccini et al., 1999). Second, using alumino-silico sources that bring Al^{3+} and Si^{4+} ions into contact at the molecular level can accelerate the formation of the $SiO_2 \bullet 2Al_2O_3$ compound, as it only requires short-range diffusion (Johnson et al., 2001; Sahnoune et al., 2008). Finally, adding special sintering additives or mineralizing agents, such as MoO_3, WO_3, AlF_3, and V_2O_5, can allow Al^{3+} ions to precipitate in the previously formed mullite nuclei, enabling the mullite grains to grow at low temperatures without the need for the liquid to be saturated by these ions (Gao et al., 2022).

Chemical methods for mullite synthesis have been developed based on chemical processes, including the sol-gel (Roy et al., 2015), spray pyrolysis (Janackovic et al., 1998), and chemical vapor deposition techniques (Haynes et al., 2004). These techniques produce fine-grained, chemically pure, and homogeneous mullite powders that can be used to create ceramics with improved high-temperature mechanical properties (L. Lima et al., 2022). While all these techniques have their own advantages, the sol-gel method is particularly advantageous because of its relatively low sintering temperature (980-1250°C), high purity, and homogeneity, which is the result of molecular-level mixing of the starting materials (Lamara et al., 2022).

Based on the level of homogeneity, sol gel methods can be divided into two types: monophasic and diphasic gels (Cividanes et al., 2010; L. Lima et al., 2022). Diphasic gel in mullite synthesis refers to a gel precursor composed of two distinct phases, alumina (Al_2O_3) and silica (SiO_2), which are homogeneously distributed or mixed at the nano level (D. W. Hoffman et al., 1984; Roy et al., 2015). The use of diphasic gels is typically favored for the synthesis of mullite ceramics, as it allows for precise control over the hydrolysis and condensation rates, which play a crucial role in determining the properties of the final material (Cividanes et al., 2010). Moreover, the incorporation of seeds into diphasic gels can promote the formation of mullite crystals, leading to high-purity and high-activity mullite powders that can be sintered to achieve a high density and strength (Hong et al., 1995).

The diphasic gels process for synthesizing mullite ceramics is recognized for its ability to produce high-purity and homogenous materials; however, it can be economically challenging because it often requires the use of expensive raw materials, such as tetraethyl orthosilicate and aluminum nitrate nonahydrate, which can increase production costs (Song, 2011; Xu et al., 2021).

Nevertheless, there studies have suggested alternative approaches to reduce costs, such as using waste as a source of silica and alumina for mullite formation. This not only lowers material costs but also provides environmental benefits by utilizing waste materials (Chen et al., 2023; Romero et al., 2021).

Mineral-rich solid wastes are among the many solid wastes that have received attention because of their potential for resource recovery and environmental sustainability, and the reclamation of minerals from solid waste aligns with the principles of the circular economy (Tejaswini et al., 2022; Yu et al., 2024). Industrial waste, mining waste, and several agricultural wastes are among these (Miao et al., 2022). Commonly known wastes include fly ash, red mud, blast furnace slag, slag/sludge, rice husk ash, and bagasse ash. In the industrial sector, one factory that contributes to solid waste in Ethiopia is Awash Melkasa Chemical Factory, in which producing 1,700 tons of useful Aluminum sulphate chemical annually, and in the meantime filter-cake waste (name of by product) is disposed of in landfills (Bereda et al., 2023). Therefore, several research have been done to address these waste using as cement replacement (Bereda et al., 2023), and extract silica using sol gel methods (Tesfaye et al., 2022).

The silica extraction process involves three primary chemical treatments: acid leaching, alkaline treatment, and silica recovery. These treatments are used to effectively separate silica from other substances (Razak et al., 2022). Acidic leaching in the context of silica extraction refers to a process in which an acid solution is used to dissolve and remove impurities from a silica-containing material, leaving behind a more purified form of silica (Pa et al., 2014). Alkaline treatment is a process that produces a Na_2SiO_3 solution from raw materials using a NaOH solution. The resulting solution containing soluble silicates can then undergo further processing, such as precipitation or crystallization, to recover pure silica (Park et al., 2021). Several methods are available for silica recovery. Based on the simplicity and efficiency of the process, hydrothermal, coprecipitation, and sol-gel techniques are the most widely used techniques for silica recovery (Razak et al., 2022). However, the cost of silica production using the sol-gel method is lower than that of other methods. Therefore, sol-gel is the most commonly used method for extracting silica (Milea et al., 2011).

In this study, silica derived from filter cake waste was used as the starting material and was synthesized using the sol-gel method. Aluminosilicate gels were then synthesized using diphasic

gel methods, facilitating the interaction of aluminum and silicate at the nanoscale. Ultimately, mullite ceramics are fabricated with a homogeneous phase, high purity, and low temperature, with excellent electrical properties.

1.2 Statement of the Problem

Currently, the world is grappling with the issues of energy demand and solid waste disposal. The ceramics industry has been a significant consumer of energy since the dawn of human civilization. This industry encompasses a wide range of materials, from traditional to advanced ceramics. Consequently, the demand for energy has risen in tandem with the development of these materials. Among these materials, mullite has emerged as a promising engineering ceramic. Although mullite can be produced using clay, it requires temperatures above 1450^0C to form single mullite phase and often results in a product of poor quality (Gao et al., 2023; Worrall, 1986). Similarly, mullite fabricated by solid state reaction from silica and alumina-rich wastes such as red mud, fly ash, and rice husk ash are cost-effective and environmentally sustainable; however, they contain trace elements that affect their properties above 1400^0C temperatures, besides their demand above 1450^0C temperature to form single mullite phase (Romero et al., 2021). Over the last two decades, chemical synthesis methods, such as sol-gel, chemical vapor deposition, and spray pyrolysis, have been developed (L. Lima et al., 2022). These methods are effective for forming pure and homogeneous products at low temperatures than conventional methods; however, the cost of the precursors is too high. Among the chemical syntheses, the sol-gel method is more cost-effective because it allows for the production of pure products at 980-1350^0C (Roy et al., 2021). The drawback of using an expensive precursor is improved using waste by synthesizing it at a level that meets the desired criteria, such as purity. To the best of our knowledge, diphasic gels have not been used for waste-driven aluminosilicate gel formation. Diphasic gels methods gives pure mullite ceramics with low temperature mulllization temperature (1200-1350^0C).

1.3 Objectives

1.3.1 General Objective

The general objective of this study is to synthesis and characterization of mullite from waste derived aluminosilicate gels for dielectric application.

1.3.2 Specific Objectives

- To prepare silica gel from silica-rich filter Cake.
- To assess the purity of silica using XRD and FTIR.
- To synthesis of aluminosilicate gels using diphasic gels.
- Fabrication of mullite ceramics from aluminosilicate gels.
- Characterize the mullite formation by using TGA/DTA, XRD, SEM/EDS, and FTIR.
- To examine mechanical and physical properties and dielectric strength.

1.4 Significance of the Study

This study achieved several significant outcomes: The energy consumption was reduced as pure and homogeneous mullite is formed at lower temperatures compared to conventional sintering methods. In addition, pure mullite can be synthesized from waste materials using suitable synthesis processes. Finally, the major drawback of chemical mullite synthesis, which is the high cost of the precursors, can be addressed using waste-derived materials.

1.5 Scope of the research

This study covers the synthesis of mullite ceramics from waste-driven aluminosilicate gels for dielectric applications. It started from preparing pure silica gel which used as starting material for silicon. Subsequently, an aluminosilicate gel was synthesized from aluminum nitrate precursors and a previously prepared silica gel via diphasic gels. Three different silica compositions were utilized in the preparation of the aluminosilicate gels to determine the optimal conditions, and determined using XRD. Subsequently, the optimal compositions underwent various characterizations including TGA/DTA, XRD, FTIR, and SEM/EDS analyses. Finally, fabricated mullite ceramics subjected to rigorous testing, including physical tests (linear shrinkage, water absorption, porosity, and density), compression strength assessment, and dielectric strength assessment.

CHAPTER 2

LITERATURE REVIEW

2.1 Overview on Mullite Ceramics

The origin of the term ceramic traces back to the Greek word “keramikos,” translating to “burnt material, “indicating the crucial role of high-temperature firing in achieving desirable properties (Callister Jr & Rethwisch, 2020). Ceramics have extensive applications in diverse fields, such as construction, manufacturing, industries, aerospace, and biomedical engineering, owing to their exceptional characteristics, such as robust mechanical strength, thermal and chemical stability, and suitability for thermal, optical, electrical and magnetic functions (Chen et al., 2019).

There are two categories of ceramics: traditional and advanced ceramics. Traditional ceramics consist of inorganic non-metallic solids, which can be either non-metallic or metallic compounds, along with clay, silica, and feldspar (Otitoju et al., 2020). Traditional ceramics have been used for centuries in a wide range of applications including pottery, bricks, tiles, sanitary ware, and porcelain. They are valued for their durability, heat resistance, and aesthetic value. In contrast, advanced ceramics are composed of oxides, nitrate compounds, carbides, and non-silicate glass. Advanced ceramics are crystalline materials with meticulously controlled compositions that are manufactured using the precise regulation of highly refined or characterized raw materials to achieve specific attributes (Belmonte, 2006; Callister Jr & Rethwisch, 2020). Advanced ceramics are commonly referred to as technical ceramics, high-tech ceramics, and high-performance ceramics worldwide. These ceramics play a significant role in a wide range of industries, sectors, and markets, and have a significant impact on them (Yan et al., 2023).

From a broad perspective, the advanced ceramic industry encompasses several categories, including functional ceramics, structural ceramics, bioceramics, ceramic coatings, and special glasses (Rödel et al., 2009; Yan et al., 2023). Functional ceramics are ceramic materials that possess specific functional properties such as electrical and magnetic properties (e.g., dielectric, piezoelectric, and ferromagnetic), ionic conductors, and superconductive ceramics. Structural ceramics are ceramic materials used in structural applications such as monoliths and composites, including oxides, nitrides, carbides, borides, and composite materials based on these materials.

Bio-ceramics, such as hydroxyapatite and alumina, are ceramic materials used in biomedical applications. Ceramic coatings are thin films applied to surfaces using technologies such as spraying, vapor deposition, and sol-gel coating, and include oxides, nitrides, carbides, borides, and diamond-like coatings. Special glasses are processed flat glass, fire-resistant glazing, and glasses for optoelectronics (Rödel et al., 2009; Yin et al., 2010).

Mullite is one of the most important oxide materials, and it conventional as well as advanced ceramics (Roy et al., 2021). Approximately a century ago, the geologists Anderson, Wilson, and Tait from the Scottish Branch of His Majesty's Geological Survey stumbled upon the first known natural occurrence of mullite while collecting mineral samples from ancient lava flows on Mull Island, located off the west coast of Scotland. Initially misidentified as sillimanite, these specimens were later recognized as mullite (Duval et al., 2008). The formation of natural mullite on the Isle of Mull is due to volcanic activity through contact with superheated lava, which produces a high-temperature mullite phase (L. Lima et al., 2022; Roy et al., 2021). Owing to its high temperature and low-pressure production conditions, it is rare to find naturally (Schneider & Komarneni, 2006).

Despite their rarity in natural rocks, mullite is one of the most important ceramic phases. Thus, the mullite phase has had a significant influence on the development of human civilization and culture, since ceramic materials have reached far back in history. Mullite ceramics are not a recent invention; in fact, they have a long history dating back to the Shang period (1500-1000 BC) in China, where they were known as "white pottery". However, the first piece of information on porcelain fabrication was recognized during the Tsang dynasty (approximately 620 AD). This early porcelain was produced from kaolin at a firing temperature of approximately 1300 C. In Europe, the first successful porcelain production was performed in Saxony (Germany) at the beginning of the eighteenth century. Mullite-bearing refractories and technical porcelains with a wide variety of special products and uses have become particularly important since the nineteenth-century industrial revolution (Schneider & Komarneni, 2006).

In addition to its significance in conventional ceramics, mullite is a strong candidate for use in advanced structural and functional ceramics (Roy et al., 2021). However, the synthesis methods also vary over time based on the application and desired properties. Previously, mullite was formed from kaolin, sillimanite, and kyanite via high-temperature sintering (Holm & Kleppa, 1966).

Currently, a wide variety of synthesis methods have been developed to meet the desired process and properties for advanced mullite ceramics. These methods include sol-gel, spray pyrolysis, hydrothermal, and vapor state processes (Lamara et al., 2022).

2.2 Structure of Mullite

Four types of anhydrous aluminosilicates are found in nature. Three of these, namely, andalusite, kyanite and sillimanite are only naturally occurring minerals and have general formula of $Al_2O_3.SiO_2$ (Al_2SiO_5) (Aksay et al., 1991; Bradt, 2008). The similarity in structure among the three sillimanite minerals is noticeable, as their structures are closely related to that of mullite. Given this relationship, all three minerals transform into mullite upon decomposition (Holm & Kleppa, 1966; Zhai et al., 2020).

The crystal structure of mullite can be described by sillimanite structure (Al_2SiO_5), as shown figure 2.1. The sillimanite structure consists of chains of octahedral groups of oxygen atoms around aluminum and runs parallel to the c-axis at each corner (Sadanaga et al., 1962). The octahedral chains in sillimanite are linked by tetrahedral T_2O_5 di-cluster groups (T = Al^{3+} , Si^{4+}), forming double chains with an ordered distribution of Al and Si atoms (Schneider et al., 2015).

Mullite has a crystalline structure closely related to that of sillimanite ($Al_2O_3.SiO_2$) and both have silicon and aluminum atoms located in tetrahedral sites. However, in the mullite structure, there is no such regularity because Si^{4+} cations can be replaced by Al^{3+}, and the compensation of the charge deficiency induced by this substitution is achieved by removing an oxygen atom that joins a tetrahedral group (L. K. S. Lima et al., 2022). This produces oxygen vacancies, according to the coupled substitution

$$2Si^{4+} + O_2 \text{------} 2Al^{3+} + \text{vacancy ([])} \quad \text{……..2.1}$$

This reaction involves the removal of oxygen atoms from the structure, leading to oxygen vacancies and the rearrangement and disordering of tetrahedral cations. Improvements in the structure revealed that the oxygen atoms connecting the two polyhedral in the tetrahedral double chain of sillimanite (referred to as O(C) atoms) are eliminated in mullite (Fischer et al., 2012). Simultaneously, the two tetrahedral cations originally linked to this O(C) site are displaced to a new position, and O(C) becomes three-fold coordinated by cations forming T_3O groups (so-called tri-clusters). It is generally accepted that tri-clusters are preferentially occupied by Al.

The octahedral AlO_6 clusters, which form a columnar structure by sharing edges, and the center of the orthorhombic unit cell does not change during this rearrangement (Schneider et al., 2008).

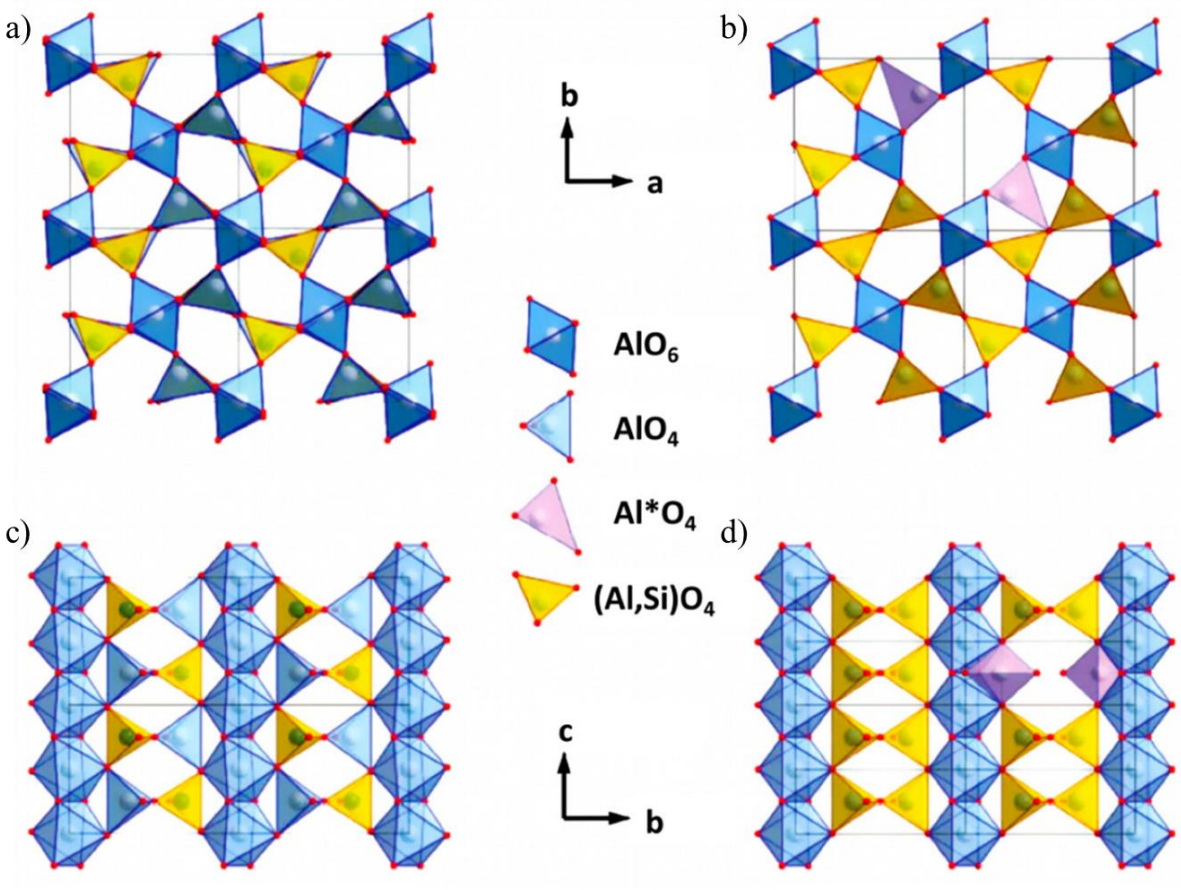

Figure 2. 1: Crystal structure of (a, c) sillimanite and (b,d) mullite (Cui et al., 2020)

In general, the elemental composition of mullite in this well-accepted defect structure is expressed as

$$Al_2^{VI}(AI^{IV}_{2+2x}\,Si_{2-2x})\,O_{10-x} \quad \ldots\ldots\ldots\ldots\ldots 2.2$$

Where x denotes the amount of missing oxygen from the formula VI and IV denote six-fold and four-fold co-ordinations of aluminum, respectively, and silicon occupies the fourfold positions (Aksay et al., 1991).

Schneider et al. (2015) provided an overview of the compositional series of mullite-type $Al_2(Al_{2+2x}Si_{2-2x})O_{10x}$ phases, highlighting distinct structural variations across different compositions. Sillimanite (x=0) is characterized by ordered AlO_4 and SiO_4 tetrahedral diclusters linking AlO_6 octahedral chains with on oxygen vacancies present. "Sillimullite" ($0<x<0.2$) exhibits similar diclusters with some oxygen vacancies. However, the exact solid-solution range of these phases remains ambiguous. Mullites with x values between 0.2 and 0.67 show di- and tri-clusters of disordered AlO_4 and SiO_4 tetrahedra linking AlO_6 octahedral chains, with increasing oxygen vacancies as x increases. Mullites with high Al_2O_3 content ($0.67 < x < 1$) likely contain tri-and tetra-clusters of disordered AlO_4 and SiO_4 tetrahedra connecting AlO_6 ocahedral chains, with a constant number of oxygen vacancies. However, the specific solid solution range for these phases are not clearly defined t-alumnia (x=1) is proposed to have tetraclusters of AlO_4 linking AlO_6 octahedral chains, although detailed crystal structure information for t-alumina remains uncertain.

Crystallographically, sillimanite and mullite have different space groups and unit-cell parameters. Sillimanite has a space group of Pbnm, whereas mullite has a space group of Pbam (Lenz et al., 2020). Sillimanite has a space group of Pbnm, which is a primitive orthorhombic space group. This space group has a fourfold axis of rotation perpendicular to the c-axis and a mirror plane perpendicular to the b-axis. The primitive unit cell of sillimanite contains two formula units, with lattice parameters of a = 7.45 A, b =7.81 A, and c = 5.68 A. In contrast, mullite has a space group of Pbam, which is a primitive orthorhombic space group with a two-fold axis of rotation perpendicular to the c-axis. The primitive unit cell of mullite contains four formula units, with lattice parameters of a = 7.65 A, b = 7.99 A, and c = 2.98 A (Burnham, 1963; Sadanaga et al., 1962; Schneider et al., 2015). Additionally, the unit cell parameters, including the lengths of the unit cell edges and the angles between them, are different for sillimanite and mullite, reflecting their distinct crystal structures and symmetries (Burnham, 1963). These differences in symmetry and crystal structure are related to the arrangement of atoms within the crystal lattice and the specific bonding patterns that give rise to the unique properties and behavior of these materials (Schneider et al., 2015). Additionally, the ordering of aluminum on the sillimanite-type $(Al,Si)^{IV}$ sites cannot be detected, and new $(Al)^{VI}$ sites can be detected by XRD and electron diffraction analysis (Aksay et al., 1991).

2.3 Synthesis Methods

Owing to its mineralogical rarity, natural mullite deposits are unable to meet the growing demand for this material. Therefore, its synthesis has become increasingly important (L. Lima et al., 2022). Furthermore, in advanced ceramics, the purity, homogeneity, mullization temperature, densification, and other mechanical, electronic, and thermal properties depend mainly on the synthesis method (Roy et al., 2021). The homogeneity of raw materials depends largely on the processing and synthesis method used, that is, how to mix, precipitate, hydrolyze, or react with SiO_2 and Al_2O_3 components (Anggono, 2005). The mechanism of mullite formation depends on the method of combining the alumina- and silica-containing reactants (Anggono, 2005). It is also related to the temperature at which the reaction leads to the formation of mullite (mullitization temperature). Mullitization temperatures have been reported to differ by up. to several hundred degrees Celsius depending on the synthesis method used (Roy et al., 2021). The preparation methods can be classified into three different routes: (1) sinter-mullite, (2) fused-mullite, and (3) chemical-mullite (high-purity mullite). The three synthesis methods used to prepare mullite are discussed in the following sections.

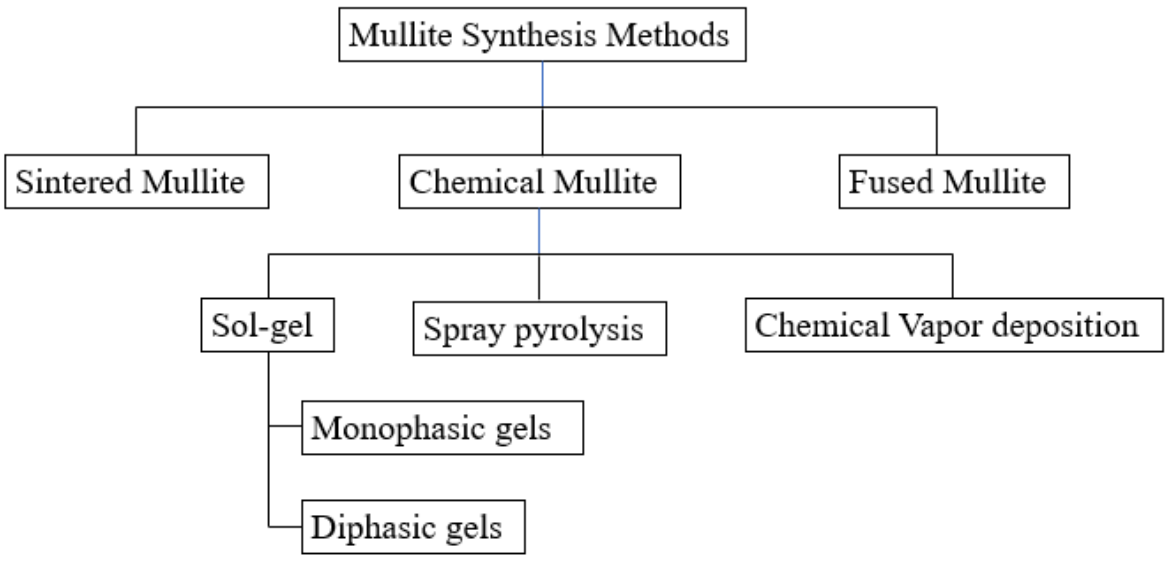

Figure 2. 2: Schematic descriptions of mullite synthesis methods

2.3.1 Sintered Mullite

Sintered mullite refers to mullite synthesized though a solid-state diffusion-controlled reaction. This process involves the diffusion of raw materials above 1450^0C, but below their melting points, resulting in the crystallization and densification of the phase (Roy et al., 2021). According to Gao et al. (2023), the process of mullitization begin at 1320 °C and terminate around 1480 °C for rare earth kaolin. Furthermore, the temperatures mentioned in (Dong, Diwu, et al., 2008) and Chen et al. (2021) indicate that mullitization occurs at approximately 1400 °C(Gao et al., 2023). The process of interdiffusion between ions commences at the interface between the alumina and silica particles as they are heated. The ions from alumina primarily diffused into the silica particles, resulting in the formation of a silico-aluminous liquid. As the temperature increases, the diffusion of ions persists, and the liquid progressively becomes more enriched in aluminum ions until the quantities of silicon and aluminum ions reach the stoichiometric proportion of the phase (L. Lima et al., 2022). Pure alumina and silica are the most commonly used starting materials for the synthesis of mullite ceramics. Clay minerals such as kaolin, pyrophyllite, polymorphs sillimanite, andalusite, and kyanite can be used as starting materials to fabricate mullite (Roy et al., 2021). Natural starting materials, particularly those rich in impurity oxides (such as Fe_2O_3, TiO_2, Na_2O, and CaO), can lead to the formation of glass phases in ceramics and refractory products. These glass phases significantly undermine the mechanical stability of these materials. This route is used to synthesize mullite primarily for refractories, crucibles, plates, bushes, and tubes, which are used in high-temperature applications (Krenzel et al., 2019).

2.3.2 Fused-Mullite

Fused-mullite refers to mullite that has been manufactured either by heating the raw materials in an electric furnace above 2000 ^{0}C, resulting in the crystallization of mullite during the cooling of the bath, or by using Czochralski crystal growth techniques (Anggono, 2005). The formation of crystallized mullite from liquids is influenced by two main factors: the temperature at which it is fired and the initial composition of the material (L. K. S. Lima et al., 2022). To attain a higher Al_2O_3 content, rapid quenching, a lower, Al_2O_3 bulk composition, or alternatively, slower cooling process can be employed (Anggono, 2005). According to Lima et al. (2022), the ratio of alumina to silica influences the mullite microstructure. To obtain acicular mullite grains, the weight ratio should be between 2.2 and 2.7. When the ratio is below 2.2, no mullite formation occurs, and when

it is above 2.7, round grains are formed. For Al_2O_3/SiO_2, weight ratios greater than 3.3, a-Al_2O_3 precipitation occurs with mullite (L. K. S. Lima et al., 2022). The raw materials used for fused-mullite ceramics and refractories are Bayer alumina, quartz sand, rock crystals, and fused silica. Fused mullite is used in many applications, such as shell building, glass contact refractories, kiln furniture, and composite (Roy et al., 2021). It also used to form composites with metals for better corrosion resistance, wear resistance, and high-temperature stability (L. K. S. Lima et al., 2022).

2.3.3 Mullite Obtained by Chemical Methods

All chemical methods to obtain mullite consist of placing Al^{3+} and Si^{4+} ions in close contact. The main methods used include: sol-gel, precipitation, chemical vapor deposition and hydrolysis (Anggono, 2005; L. K. S. Lima et al., 2022; Roy et al., 2021).

These techniques yield fine-grained, chemically pure and homogeneous mullite powders (Krenzel et al., 2019). Mullite coatings, films, and powders are prepared using this method, and are mostly used for advanced applications (Roy et al., 2021). Chemical methods have several techniques for mullite synthesis including:

2.3.3.1 *Spray Pyrolysis*

This method consists of ultrasonic atomization of starting solutions, sols, or suspensions, and the introduction of the generated aerosols into the reactor (furnace) at elevated temperatures (Janaćković et al., 1996). During spray pyrolysis, aerosol droplets are transformed into microporous or dense particles by different processes, including solvent evaporation, precipitation of dissolved precursors, drying, thermolysis of precipitated particles, and sintering. Because of the high heating rates, the homogeneity of the initial solution remained in the obtained particles. The advantage of this method is that all the processes mentioned above occur in one step, each droplet/particle undergoes the same reaction conditions, and no subsequent milling is necessary (Ma et al., 2014). Therefore, it is considered an appropriate preparation method for the synthesis of mullite ceramics (Janackovic et al., 1998; Janaćković et al., 1996).

2.3.3.2 Chemical Vapor Deposition Method

(CVD) is an essential method for the synthesis of mullite powder, films, and coatings. This method uses a vapor phase process to fabricate mullite (Roy et al., 2021). CVD has several distinct

advantages in the fabrication of protective mullite coatings. These include the capability to fabricate dense, high-purity crystalline mullite coatings (Haynes et al., 2004). Furthermore, this process generally results in dense coatings that can be synthesized well below the melting or sintering temperatures of the material, with the possibility of microstructural and morphological optimization through variations in the process parameters (Mulpuri & Sarin, 1996). The starting precursor molecules are typically metal-organic compounds containing aluminum and silicon, such as aluminum chloride ($AlCl_3$) or alkoxide ($Al(OR)_3$) and silicon tetrachloride ($SiCl_4$) or alkoxides ($Si(OR)_4$).

2.3.3.3 Sol Gel Synthesis Methods

Since the 1970s, when the sol-gel method was developed, numerous studies have been conducted on the raw materials used in ceramics (Won & Siffert, 1998a). Due to the significant interest among researchers in preparing mullite from chemically synthesized precursors, sol-gel methods have been widely utilized to create mullite powders, fibers, and bulk samples at relatively low processing temperatures (Anggono, 2005). The sol-gel process for obtaining the mullite phase consisted of a mixture of colloidal particles of alumina and silica, aiming for contact with the species at the nanometric level. Colloidal particles or molecules in suspension (sol) are subjected to chemical changes that cause them to unite in a continuous network, forming a homogeneous and reactive gel (L. Lima et al., 2022). Employing the sol-gel method enables the production of mullite with a homogeneous submicronic microstructure. The particles in this method are measured in the nanometer range, whereas the particles in the sintered and fused synthesis method are in the micrometer range (Roy et al., 2021). Since the 1980's this technique has been used for advanced ceramics because it allows the synthesis of mullite at low temperatures in the range of 1200- 1300^{o}C (Pask et al., 1987).

In comparison, the sol-gel technique offers several benefits over alternative methods. First, it yields high-purity ceramics due to prior purification steps such as distillation or recrystallization, which are deemed crucial for liquids or alkoxides. Second, ceramics at relatively low energy and synthesis temperatures.

Finally, the method allows for the preparation of diverse materials, such as thin films, coatings, and fibers, as it offers precise control over reaction conditions (Cividanes et al., 2010; Won & Siffert, 1998b). In conclusion, using the sol gel process, products with better homogeneity and

purity can be expected at relatively lower temperatures (between ~980 and 1350^{o}C) than those required for traditional processes (temperature 1450-1800^{o}C) (Roy et al., 2015).

2.4 Sol Gel Methods

The term “sol-gel” was introduced by Graham in 1864 while he was conducting research on silica sols. In 1640, va helmont had discovered “water glass” by dissolving silicate materials in alkali and subsequently precipitating silica gel upon acidification (Ciriminna et al., 2013). In the mid19th century, Ebelman reported the formation of a transparent substance through the gradual hydrolysis of ester derived from silica acid (Dimitriev et al., 2008).). In 1930, researchers Geffcen and Berger from Shott company developed a sol-gel process for formation of oxide layers on industrial glasses using precursors containing metals. They also created single oxide coatings using this method (Dislich & Hinz, 1982).).

This innovation open for pioneering research, such as creation of non-crystalline substances with strong chemical bonds between organic and inorganic elements (Schmidt, 1985), incorporating organic dye in oxide gels, which led to the development of nanocomposites (Avnir et al., 1984),), low temperature synthesis of ceramics material, and the first practical achievement associated with preparation of fiber, coating and monolithic products as shown figure 2.3 (Dislich, 1971).

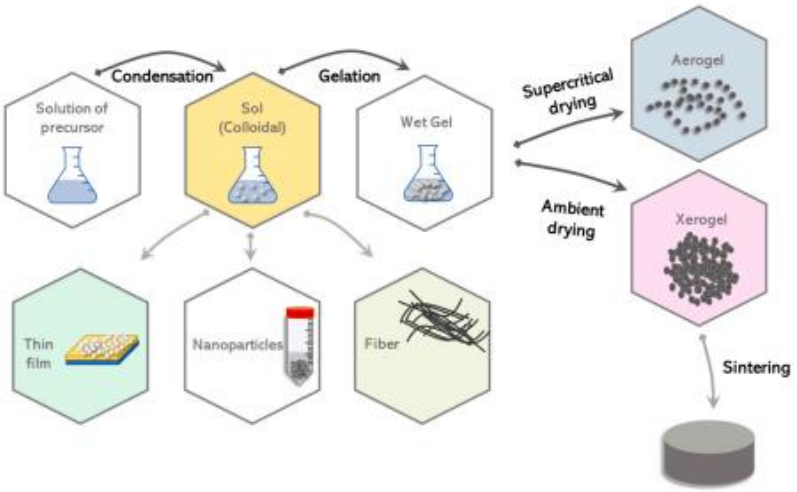

Figure 2. 3: Representative image of different products obtained using sol-gel processing (Adopted from (Catauro & Ciprioti, 2021))

A sol is a suspension of solid particles in a liquid, and it can be transformed into a gel by maintaining the appropriate reaction conditions. After drying and grinding, the resulting gel can then be converted to powder. This type of powder preparation technique is termed as “sol-gel” method (Roy et al., 2015). The sol-gel process encompasses various routes or pathways that can be tailored to produce a wide range of materials with diverse properties and functionalities (Ciriminna et al., 2013). These routes differ in the choice of the starting materials, reaction conditions, and processing steps, allowing the flexibility in the material synthesis. Hydrolysis and condensation of metal alkoxides , colloidal dispersion, non-hydrolic sol-gel reactions, pechini gel methods(Chelate polystirication), polymer pyrolysis ,and inorganic-organic hybrid these are several routes of sol-gel processing (Cassidy et al., 1997; Dimitriev et al., 2008). Metal alkoxoide are popular metal oxides ceramic precursors because of the purity of the starting materials, low temperature at which the reaction occur, the ease of the reactions, and their reactivity toward water (Bokov et al., 2021).

Essentially, two governing reactions are involved in the metal alkoxide method: hydrolysis and condensation (Bokov et al., 2021; Hu et al., 2000).In the first step of the sol-gel process, metal alkoxides react with water (H_2O) to undergo hydrolysis. This reaction involves the breaking of the metal-oxygen bonds in the alkoxide group and the formation of metal hydroxide (M-OH) groups. The formation of a sol, a stable suspension of colloidal particles in a liquid, in the initial stage occurs as following equation (Catauro & Ciprioti, 2021)

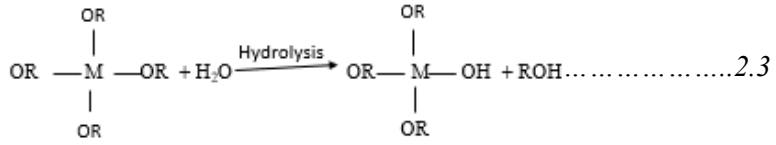

2.3

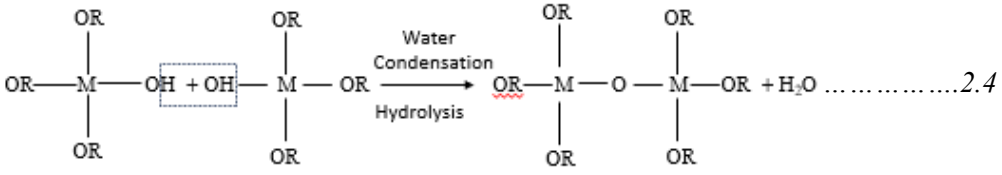

2.4

In the subsequent step, the metal hydroxide species formed via hydrolysis undergo condensation reactions, leading to the formation of metal-oxygen-metal (M-O-M) linkages as shown in equation 2.4. These linkages result in the formation of a three-dimensional network structure, known as a gel, composed of metal oxide (M-O-M) bonds (Schmidt & Scholze, 1985; Schmidt et al., 1984). Gelation largely depends on factors such as (i) degree of homogeneity (ii) extent of hydrolysis and condensation, and (iii) pH of the medium (Roy et al., 2015).

The sol-gel method is highly versatile due to its capacity to regulate the chemical composition, structure, and properties of the final materials by precisely adjusting the synthesis parameters, including precursor concentration, solvent blend, the addition of organic and inorganic additives, pH, and temperature (Cividanes et al., 2010; Parashar et al., 2020). The use of this control mechanism permits the customization of materials with specific functionalities and properties, thereby establishing sol-gel synthesis as a vital technique for the development of advanced ceramics (Innocenzi, 2023).

The sol–gel method has been widely used for mullite synthesis, generating products with high purity and homogeneity. According to the gel homogeneity degree, sol–gel method is divided into two types (Cividanes et al., 2010; L. K. S. Lima et al., 2022):

2.4.1 Monophasic gels

Monophasic gels are crucial in the sol-gel synthesis process of mullite, as they ensure a homogeneous mixture of aluminum and silicon at the atomic level, resulting in uniform precursor solutions. (Nair et al., 2024). Monophasic gels form through the substitution of silicon from the three-dimensional silica network with atoms or hydrolyzed aluminum molecules. De Sola et al. (2006) stated that there are two primary methods for preparing single phase gels. The first method, known as all alkoxide, is based on the controlled hydrolysis of aluminum and silicon alkoxides. The second method, named semi-alkoxide, utilizes a salt of aluminum, typically nitrate nonahydrate. It is challenging to manage reactivity when using all-alkoxides because of the very different hydrolysis rates of aluminum and silicon alkoxides, resulting in some heterogeneity. However, the semi-alkoxide method achieves greater homogeneity, as demonstrated by the formation of mullite at approximately 1000 ◦C at a lower temperature (de Sola et al., 2006). This process leads to the formation of Al-O-Si bonds, which are similar to those observed during mullite crystallization. (Cividanes et al., 2010).

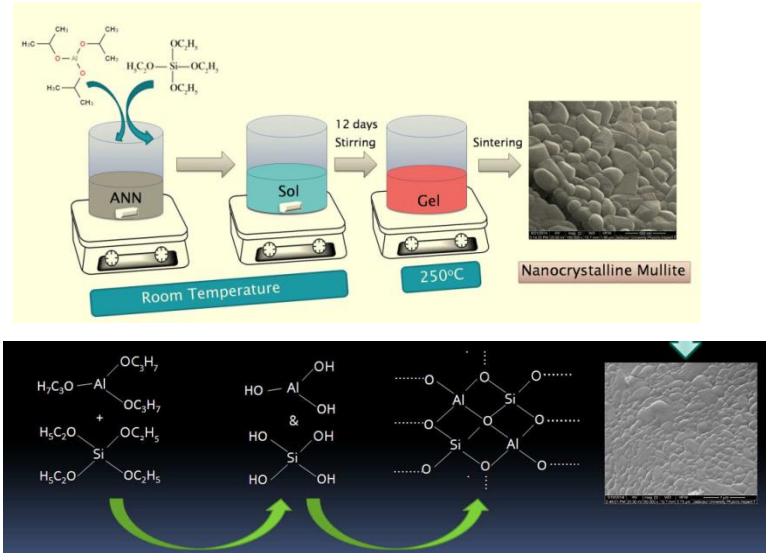

Figure 2. 4: Schematic diagram of mullite synthesized from monophasic precursor(Kool et al., 2016)

The formation of monophasic gels entails the controlled hydrolysis and condensation of metal alkoxides like tetraethyl orthosilicate (TEOS) and aluminum nitrate nonahydrate (ANN) (Jaymes et al., 1996). Notably, monophasic gels possess a unique characteristic that they have the ability to directly crystallize orthorhombic mullite (the more stable phase of mullite) at relatively lower temperatures bypassing the formation of intermediate phases. This specific crystallization behavior simplifies the synthesis process and ensures the purity of the final mullite material by eliminating unwanted intermediary phases (Li & Thomson, 1990).

2.4.2 Diphasic gels

It is a material forming process with two or more phases interactions, where the physical dimensions of these phases are range from 1 to 100 nanometers. The two phases may differ in either their composition or structure, or both. (D. Hoffman et al., 1984). Hoffman initiated the synthesis of mullite diphasic gels, by sol–gel process in 1984, and used aqueous silica sol and boehmite sol as starting materials. The reason behind mullite formation at low temperature is the rate of mullite formation increases as the particle size of the sample mixture decreases (Li & Thomson, 1990). Li and Thomson (1990) explained that mullite formation in diphasic gels usually follows a nucleation and growth pattern, but this process is limited by diffusion mechanisms, especially the transport of reactants to the growing interface of mullite particles. The authors

suggested that if Al_2O_3 and SiO_2 could be combined at the molecular level, the temperature required for mullite formation could be reduced, resulting in shorter diffusion paths and potentially making the kinetics of mullite formation less dependent on diffusion.

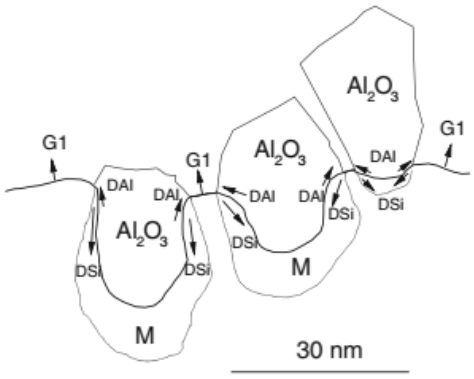

Figure 2. 5: Schematic plot of partially reacted Al_2O_3 particles on the mullite/Al_2O_3/Si02 interface (WEI & Halloran, 1988b).

In 1988, wei and halloran (1988) examined phase transformation and mullite formation in aluminosilicate gels (fig 2.5). The research of authors led to the development of a model for the crystallization process, which is based on the formation of a mullite interface between the alumina and silica grains. The growth mechanism of this process was controlled by the diffusion of silicon and aluminum in this interface (WEI & Halloran, 1988b). The mullite formation mechanism, in the case of diphasic precursors it has been found that the growth rate of the mullite grains is controlled by dissolution of the alumina particles into the amorphous silica-rich phase (Sales & Alarcón, 1996).

The primary benefit of employing diphasic gels lies in the potential to compact powder formations by leveraging the flow properties of the amorphous silica at temperatures below -1250°C, prior to the onset of mullitization. Subsequent heat treatment above 1250°C enables the formation of a crystalline mullitic microstructure. Referred to as the transient-viscous-sintering or glass-ceramic route, this method has been adopted by numerous researchers to produce mullite ceramics characterized by fine, uniform, and isotropic microstructures (Boccaccini et al., 1999). Furthermore, the main advantage of a diphasic gel system over a monophasic one is that the heat generated by the reaction between the different phases helps to facilitate the densification process (Roy et al., 2015).

Table 2. 1: Summary on comparison between monophasic and diphasic gels

Parameter	Monophasic	Diphasic	Reference
Phase	• The phases of precursors are single	• The phases of precursors are two or more (ex. gel and sol)	(Cividanes et al., 2010; L. Lima et al., 2022; Roy et al., 2015)
Homogeneity of precursors	• Aluminum and silicon are mixed at the atomic level	•The homogeneity scale between aluminum and silicon is between 1 and 100 nm.	(Cividanes et al., 2010; L. Lima et al., 2022; Roy et al., 2015)
Mullization temperature	• Mullite crystallization occurs at a temperature of approximately 980 °C	• Mullite crystallization occurs at temperatures close to 1300 °C	(Cividanes et al., 2010; L. Lima et al., 2022; Roy et al., 2015)
Phase transformation	• Without formation of intermediate phases	• A transient phase formation usually occurs before the mullite crystallization • At >1200^{0}C from mixtures of an amorphous silica-rich phase and a poorly crystalline high-alumina (-6Al203. Si02) phase commonly referred to as spinel.	(Cividanes et al., 2010; Huling & Messing, 1991; L. Lima et al., 2022)
Activation Energy	• The activation energy of crystallization process for mullite varies from 300 to 400 kJ/ mol	• Higher activation energy (~1000 kJ/mol) are required for mullite crystallization	(Cividanes et al., 2010; L. Lima et al., 2022; Roy et al., 2015)
Rate of hydrolysis	• Monophasic gels can be formed through slow hydrolysis of alkoxide and saline solutions.	• Diphasic gels can be formed through rapid hydrolysis of alkoxide or saline solutions.	(Cividanes et al., 2010; L. K. S. Lima et al., 2022)

2.4.3 Commercial starting material for sol gel methods

Many researchers used diverse starting materials to synthesis mullite through sol gel methods. The starting materials include Tetraethylorthosilicate (TEOS) and aluminum nitrate nonahydrate (ANN) (Chen et al., 2022), TEOS and aluminum isopropoxide (AIP) (Jana & Ray, 2020), TEOS and pseudoboehmite (WEI & Halloran, 1988a), TEOS and boehmite (Li & Thomson, 1990), ANN and colloidal silica (Lee et al., 2002), fumed silica nanopowder and boehmite sol (Boccaccini et al., 1999), commercial mullite powder (Johnson et al., 2001; D. Liu et al., 2020), aluminum carboxylates and silica sol (Tan et al., 2010). However, ANN and TEOS have been found to be the most popular precursors after Rustum Roy used these two for mullite synthesis first time in 1958 (Roy et al., 2015). Silica sources are one of main important factors for mullite synthesis.

Silicon is the most abundant element in the earth's crust after oxygen, and shows a rich variety of chemical properties and it lies at the heart of much modern technology ("9 - Silicon," 1997). Even though it is abundant in nature as Quartz and elemental silicon, it is not ideal silica sources for sol-gel methods due to low reactivity, insolubility in solvents, lack of control over hydrolysis and condensation reactions, and processing challenges.

In contrast, tetraethyl orthosilicates are the preferred choice for sol-gel processes due to their reactive alkoxide groups, solubility in solvents, and their well-defined molecular structure. These characteristics make them ideal for use in sol-gel processes (Bokov et al., 2021).

The production of silica sources, including colloidal silica, sodium silicate, and tetramethyl-orthosilicate, involves the use of quartz and sodium silicate at elevated temperatures. Common methods such as Thermochemical or fusion methods (Vinai & Soutsos, 2019), direct oxidation (Hyung Mi et al., 2010), alkaline fusion, and reactive distillation column (Sánchez-Ramírez et al., 2018) have been utilized for this purpose. However, a significant drawback of existing methods is the requirement of high-temperature calcination, reaching up to 1710°C, which poses challenges in silica production. Additionally, the large-scale production of crystalline silica nanoparticles may lead to the release of toxic substances into the working environment, creating unsafe conditions that could result in occupational diseases such as lung cancer and pulmonary tuberculosis (Tessema et al., 2023).

In addition, another source of silica that has been used for the synthesis of mullite precursors is silicic acid, or an aqueous silica suspension. This route allows lower costs compared to the one that uses TEOS as a source of silica, however, it is not yet the most used (L. K. S. Lima et al., 2022).

2.5 Wastes utilization as starting material for mullite synthesis

Numerous investigations have been conducted to develop mullite ceramics using various precursors, ranging from naturally occurring aluminosilicate minerals to industrial/laboratory grade chemicals (Romero et al., 2021). As a result of its scarcity in nature (L. Lima et al., 2022) and the high cost of its starting materials, which are typically synthesized (de Brito et al., 2021), researchers have been actively seeking cost-effective methods for the production of mullite ceramics for several years. Hence, mining waste (Romero et al., 2021), industrial waste (Choo et al., 2019), and agricultural waste (Hossain et al., 2020) have been investigated as potential starting material for mullite.

Mining wastes, industrial wastes, and agricultural wastes are considered as starting materials for mullite ceramics due to their rich content in silica (SiO_2) and alumina (Al_2O_3), which are essential compounds for manufacturing mullite ($3Al_2O_3{\cdot}2SiO_2$) (Karhu et al., 2019) (Choo et al., 2019). Additionally, the reasons mining wastes are considered as starting materials for mullite ceramics, their availability and the presence of necessary oxides (Romero et al., 2021). However, mullite formation temperature and purity or the formation of single mullite phase are one of challenge faced every research which worked on waste derived mullite ceramics. According to Gao et al. (2022), the cost of producing fly ash-derived mullite increases when aluminum sources and sintering additives are added, along with a high synthesis temperature. Additionally, it is not possible to completely avoid impurities during the synthesis process. On the other hand, the authors described that adding special sintering additives or mineralizing agents, such as MoO_3, WO_3, AlF_3, and V_2O_5, could solve the problems of high synthesis temperature and difficult mineral phase transformation. While this approach was effective in achieving the desired phases, it was not cost-effective and resulted in a product that was not highly pure (Gao et al., 2022).

Table 2. 2: Summary of mullite synthesized from different waste via solid-state sintering

Starting materials	Mullization Temperature/ Holding time	Secondary Phase	Observation	Reference
Red mud+ Kaolin	1400-1500^{0}C for 60min	Alumina	The increase in temperature caused an increase in the intensity of the mullite peaks and a decrease in the corundum peaks, indicating an increase in the solubility of mullite at high temperatures.	(da Silva et al., 2016)
Coal gangue + high alumina refractory solid wastes	1300-1400^{0}C for 3hrs	Zirconia and impurity substance	There were also secondary phases in the mullite powders, due to the impurities in the coal gangue powder	(Y. Liu et al., 2020)
Granitic sand + Reactive alumina	1450-1600^0 for 30min	Alumina	As temperature rise to 1600, it was evidenced the disappearance of residual crystalline phases, mainly quartz and cristobalite, with relicts of a-alumina in a single case.	(Sánchez-Soto et al., 2018)
Quartz waste + Alumina	1100-1300^{0}C for 3hrs	Alumina	Corundum peaks were the highest for mixture of the highest boehmite addition, thus unreacted corundum was retained in the structure.	(Karhu et al., 2019)
Fly ash + Alumina	1200-1600^{0}C for 4hrs	Corundum	Mullite becomes the sole crystalline phase after samples fired at 1400°C.	(Dong, Feng, et al., 2008)

Kaolin waste + Alumina	1200-1600^{0}C for 2hrs	Alumina or corundum	Complete mullitization (i.e., mullite as a single phase) was not achieved under these experimental conditions.	(Sánchez-Soto et al., 2022)
Schists waste + Alumina	1100-1200^{0}C	Hercynite and Hematite	The irreversible formation of hercynite, mullite and amorphous silica at above 1100^{0}C. These happened due to significant amount of iron impurity, and Iron and alumina present at close points of the same ``phase''	(Vieira et al., 1999)
Slake waste + Alumina	1250-1450^{0}C for 2hrs	Alumina and hercynite	A trace amounts of wastes at 1450 C it changed into glass phase and not detected under XRD however above 1450^{0}C there is bubble formation due to decomposition of volatile components	(Oliveira et al., 2008)
Rice husk ash + Alumina	1200-1500^{0}C for 5hrs	Alumina	A higher Al_2O_3 content with the dissolution of amorphous silica promotes the crystallization of mullet at higher temperature.	(Wahab et al., 2017)
Sago waste + Alumina	1100 – 1700^{0}C for 2hrs	Cristobalite + Alumina	The mullite phase can be formed at a temperature as low as 1100^{0}C. It was found that a complete mullitization takes place for the composition of 40 mol% α-Al_2O_3 sintered at 1600 ^{0}C.	(Aripin et al., 2015)

2.5.1 Different types of waste derived mullite synthesis methods

The method of synthesis plays a vital role in determining the extent to which raw materials, such as alumina and silica, are mixed together (Hossain et al., 2018). The level of mixing can have a significant impact on the nucleation kinetics of mullite, which influences the temperature at which mullitization occurs and the properties of the final product (Aksay et al., 1991). For instance, in minerals processing, relatively coarse (micrometer-range) powders are used; thus, high temperatures (>1700°C) are required to complete the solid-state reactions. Despite the high temperatures, most of solid wastes often contain high impurity levels (iron oxide, titanium oxide, potassium oxide...etc.) that are unacceptable in advanced ceramic applications. Dong et al. (2008) successfully synthesized mullite from natural mineral bauxite and industrial waste fly ash. The process of mullite formation began at 1300°C, but secondary phases such as corundum and cristobalite were also present. After a 4-hour treatment at 1500°C, a single phase of mullite was formed. The process of mullization in this study involved the dissolution of waste-derived alumina into a liquid glassy phase that was formed from the melted fly ash due to the action of different metal oxide impurities (Krenzel et al., 2019). This process is referred to as secondary mullization. Despite the formation of mullite, volume expansion occurred while the liquid glassy phase promoted sintering (Dong, Feng, et al., 2008).

In contrast, in chemical processing, the intimacy of mixing dictates the mullitization temperature and phase purity in the final product. If the homogeneity is at the atomic level (‘‘single phase’’), as in chemical vapor deposition (CVD), spray pyrolysis, monophasic gels and polymer precursor methods, direct mullitization can be observed at ~980°C (L. Lima et al., 2022). On other hand, if the homogeneity is in the nanometer-to-micrometer range (‘‘colloidal’’ or ‘‘diphasic’’), mullitization occurs through a transient Al_2O_3 phase and is often evidenced by a second exotherm at a temperature >1200°C (Kansal et al., 1997). Hossain et al. (2020) managed to synthesize mullite at a relatively low temperature, specifically above 1250 °C, using RHA derived sol through the slip-casting process. The conversion occurred through the diffusion-reaction of Al3+ ions from alumina to nano-silica, which increased the number of diffusion sites for the ions and reduced the diffusion distance due to the low volume of silica particles. As a result, the activation energy for mullite formation may have been decreased, facilitating the process at lower temperatures (Hossain et al., 2020).The various types of synthesis methods are summarized in the table below.

Table 2. 3: The review of different synthesis method for mullite from waste

Starting material	Synthesis Methods	Mullization Temperature and time	Advantages of synthesis methods	Reference
Industrial waste silica + Alumina	Transferred arc plasma (TAP) processing	1400 ^{0}C for 4hrs	It is an economic and time saving processing method	(Yugeswaran et al., 2011)
Rice husk ash + active alumina	Slip- casting	1300 ^{0}C for 2hrs	It is capable to produce low-temperature in-situ mullite foam without generating the pollutants (mainly $CO_2\uparrow$).	(Hossain et al., 2020)
Slate wastes + aluminium-rich sludges	Sintering	1300 ^{0}C for 30min	It is easy, but it is difficult to synthesis single phase mullite at low temperature	(Vieira et al., 2007)
Aluminous-rich mine waste + Alumina	Thermal plasma process	treated in a high temperature plasma furnace of 50 KW power for 5minutes duration.	It is cost effective and minimal time duration	(Pani et al., 2015)
Rice husk ash + Aluminum nitrate nonahydrate	Sol gel	1350^{0}C for 6hr	It is used to synthesis single phase mullite at low temperature.	(Sembiring et al., 2014)
Rice husk ash + alumina	3D printing and firing	1400^{0}C	It is a simple and effective way to fabricate mullite foamy structure	(Hossain et al., 2022)

2.6 Ceramics for Dielectric Material

Dielectric materials are insulating substances that exhibit the ability to be polarized by an electric field, which means they can store electrical energy by aligning their dipoles in response to the field. They are integral to the functioning of capacitors, where they are placed between conductive plates, allowing the capacitor to store a greater amount of electrical charge for a given volume without conducting electricity (McLean, 1967; Nketia-Yawson & Noh, 2018). The performance of dielectric materials is not uniform across all applications; it varies with factors such as mechanical flexibility, temperature stability, and energy density. For instance, polymer-based dielectrics are being developed for their high capacitance and mechanical flexibility (Nketia-Yawson & Noh, 2018), while ceramic-based dielectrics are favored in energy storage applications due to their high power density and temperature stability (Pattipaka et al., 2024). Conventional oxide based dielectrics, such as silicon dioxide, aluminum oxide, and hafnium oxide have been widely used to achieve the desired functionality due to their high film density, relatively large capacitance and low leakage current density (Nketia-Yawson & Noh, 2018).

Ceramic materials with high dielectric constants and low losses at high frequencies that are electrically and thermally stable are suitable for applications in ceramic capacitors for energy storage (da Silva et al., 2019). Mullite ceramics are utilized as dielectric ceramics, as evidenced by the research findings across multiple studies. The dielectric properties of mullite ceramics are a focal point of investigation due to their potential applications in electronic devices. For instance, Fuertes et al. (2020) highlights that cordierite-mullite ceramics processed by Ceramic Injection Moulding (CIM) exhibit improved dielectric behavior, which is crucial for electronic applications (Fuertes et al., 2020). Similarly, USHIFUSA et al. (1990) and Ushifusa et al. (1992) discuss mullite's low dielectric constant and thermal expansion coefficient, making it suitable for substrate applications in electronics (USHIFUSA et al., 1990; Ushifusa et al., 1992). Zhang et al. (2019) further supports this by demonstrating the stable dielectric constant and low dielectric loss of porous mullite ceramics at elevated temperatures, suggesting their suitability for radome applications (B. Zhang et al., 2019). Biswal et al. (2021) presents synthesized mullite materials with high dielectric constants and low loss factors, indicating their appropriateness for electronic-related applications (Biswal et al., 2021b).

However, it is important to note that the dielectric properties of mullite ceramics can vary significantly depending on the composition and processing methods. For example, Liu et al. (2020) indicates that the sintering temperature can influence the microstructural and mechanical properties of mullite ceramics, which may, in turn, affect their dielectric characteristics (D. Liu et al., 2020).

The performance of mullite ceramics for dielectric and electronic application are mainly identified by using AC impedance spectroscopy. The important parameter to calculate the dielectric materials are dielectric constant, dissipation factor, volume resistivity and dielectric strength. The below table is standard specification for Alumina ceramics for electrical and electronic applications. Ceramics covered by this specification shall be classified by alumina content as follows: 82% alumina (type I), 93% alumina (type II), 97% alumina (type III), and 99% alumina (type IV).

Table 2. 4: Electrical requirements for dielectric application

Property	Type I	Type II	Type III	Type IV
Dielectric constant, max 25°C:				
at 1 MHz	8.8	9.6	9.8	10.1
at 10 GHz	8.7	9.6	9.8	10.1
Dissipation factor, max 25°C:				
at 1 MHz	0.002	0.001	0.0005	0.0002
at 10 GHz	0.002	0.001	0.0005	0.0002
Volume resistivity, min Ω·cm:				
at 25°C	10^{14}	10^{14}	10^{14}	10^{14}
at 300°C	1×10^{10}	1×10^{10}	1×10^{10}	7×10^{10}
at 500°C	4×10^{7}	2×10^{7}	8×10^{7}	1×10^{8}
at 700°C	4×10^{6}	2×10^{6}	6×10^{6}	1×10^{7}
at 900°C	4×10^{5}	2×10^{5}	8×10^{5}	1×10^{6}
Dielectric strength:				
3.175 mm (0.125 in.) min kV/mm	9.85 (250 V/mil)	9.85 (250 V/mil)	9.85 (250 V/mil)	9.85 (250 V/mil)

Source: ASTM D 2442 – 75

2.7 Research Gap

Previous research has been conducted on the utilization of mineral-rich wastes, such as those containing alumina and silica, as starting materials for the synthesis of mullites. These wastes can be obtained from agriculture, mining, and industrial sources. Examples of such wastes include fly ash, red mud, and slate wastes. While solid-state reactions are a common synthesis method for

mullite, advanced techniques such as transfer arc plasma, slip casting, sol-gel method (monophasic gels), thermal plasma process, and 3D printing and firing have also been employed. The effectiveness of these methods is evaluated based on factors such as mullite formation temperature and time, as well as purity. However, these methods have limitations such as poor quality, prolonged sintering times, and high energy consumptiion. No research has been conducted on the use of filter cake waste for mullite synthesis. Furthermore, although diphasic gels are commonly used for synthesizing mullite from commercial starting materials, they have not been utilized for synthesizing mullite from waste materials.

CHAPTER 3

MATERIALS AND METHODS

2.8 Equipment and chemicals used throughout the research

In this research, mullite-based ceramics were successfully synthesized utilizing sol-gel techniques. The raw materials used in this study were a combination of both commercial and waste-derived sources. Aluminum nitrate nonahydrate (Alpha Chemica) was procured from commercial sources, while silica was extracted from a solid waste material with high silica content, which was obtained from Awash Melkasa Chemical Factory.

2.9 Preparation of silica gel

This study utilized high silica content solid waste derived from a nearby Awash Melkasa Chemical Factory which is residue of aluminum sulfate product, which employs kaolin as a raw material with sulfuric acid to produce aluminum sulfate. The waste is disposed in the surrounding environment and cause problem to the ecosystem. In this research, the filter cake waste was considering as a source of silica gel. The process began with the collection and drying in an oven, then treated with HCl to remove impurity. Acid treatment is key step to purify the silica extraction. The treated waste was washed and dried then followed by calcination at 850 °C for 2 hours. Subsequently, the calcined product was ground using a mortar and pestle, yielding a fine powder ready for the basic leaching steps. In this procedure, a 1:1 ratio of solid waste to NaOH was prepared. Initially, NaOH was dissolved in distilled water, and it was uniformly mixed on a hot plate using a stirrer bar. The ground powder was then added to the solution, and the mixture was continuously stirred at 100 °C for 4 hours. During this extensive stirring process, sodium hydroxide reacted with the silica present in the waste, forming sodium silicate solution in the form of a filtrate. Then the residue was removed after filtration using filter paper. Silica recovery could be done by using sol gel methods, and HCl used to condense silica gel. This silica recovery take place at the value of 3 pH. Finally, the gel was washed several times to removes salt, and the wet gel is covered and kept for later use.

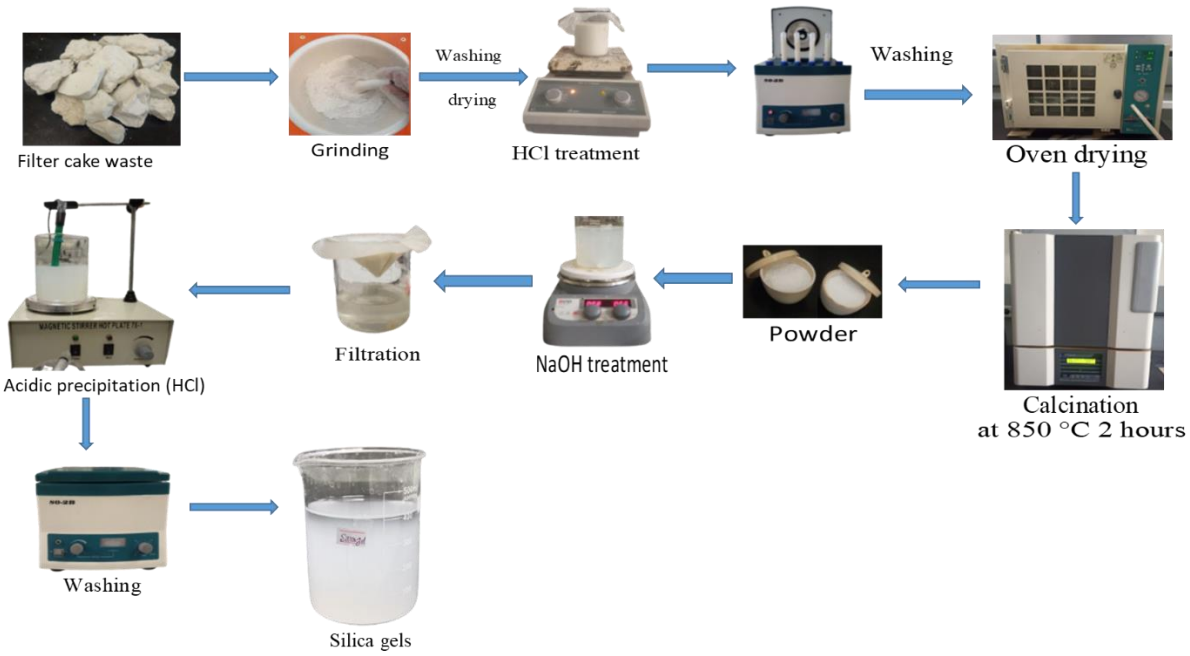

Figure 3. 1: The synthesis of silica gel from filter cake waste using sol gel methods

2.10 Synthesis of aluminosilicate gels

Using diphasic gels process by sol gel methods, aluminosilicate gels was successfully synthesized (Lee et al., 2002). The pre-prepared silica gel, aluminum nitrate (nonahydrate), distilled water, and sodium hydroxide was utilized as initial materials. Mass of the starting materials was measured using a highly sensitive electronic balance with four-digit sensitivity. First of all, 30 g of aluminum nitrate dissolved in 200 ml distilled water. The solution was stirred vigorously at room temperature until it became transparent. Subsequently, the prepared silica gel was added into the aluminum solution based on designed batch composition. Then it is stirred on hot plate for 24hr at 60^0C. the initial pH value of diphasic mixture is 2 and a 2M of sodium hydroxide solution added to form gel at 9 pH. The solution was magnetically stirred for 40 minutes to allow complete evaporation and the formation of a sol-gel solution (Mohammed et al., 2020). The mixture was centrifuged for 30-40 minutes to wash and remove salts. Finally, the gel was put into oven to dry at 120^0C for 12 hr, and form aluminosilicate powder. The white powder was eventually collected and then ground using a mortar and pestle, the powder sieved with 100 mesh size and calcine at 600^0C (Keziz, Rasheed, et al., 2023).

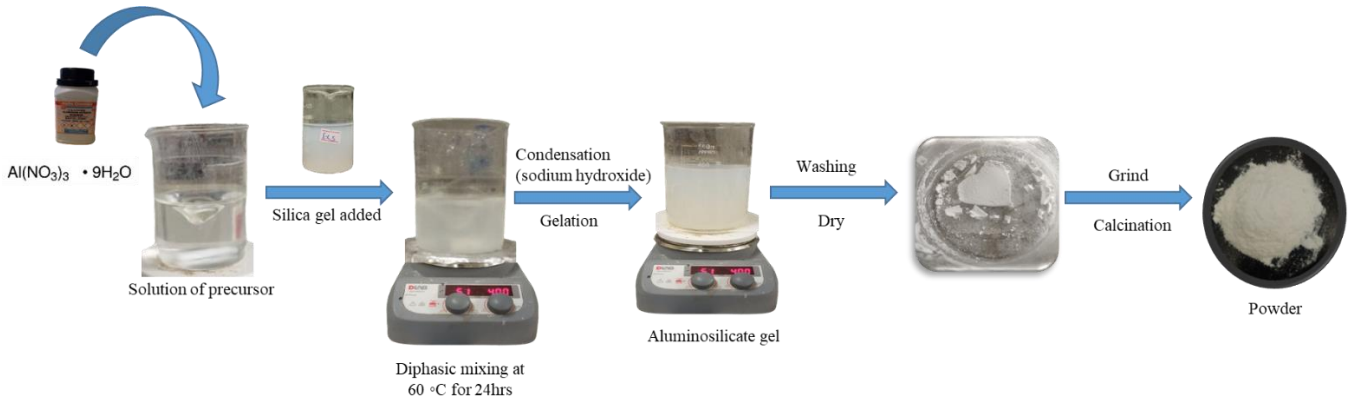

Figure 3. 2: Synthesis of aluminosilicate gels powder

2.11 Fabrication of ceramics

Mullite are typically manufactured through a series of steps, beginning with the measurement of 2 grams of dried gel powder using an analytical scale. Next, the powders were compacted to disk shapes with the pressure of 20 MPa in a steel pellet (11.6/20 mm in diameter). In ceramics, a green body refers to the unfired, shaped object made from a mixture of ceramic powder and binder. It represents the intermediate state of a ceramic component prior to sintering or firing, which results in a dense, solid form (Gupta, 2016). The selection of heating or sintering schedules was based on TGA/DTA results and aimed to ensure a solid-state reaction of a diphasic specimen. To achieve this, the mixtures were sintered in air temperatures ranging from 1150°C to 1350°C with 10°C heating rate (Schmidt et al., 2019; WEI & Halloran, 1988a).

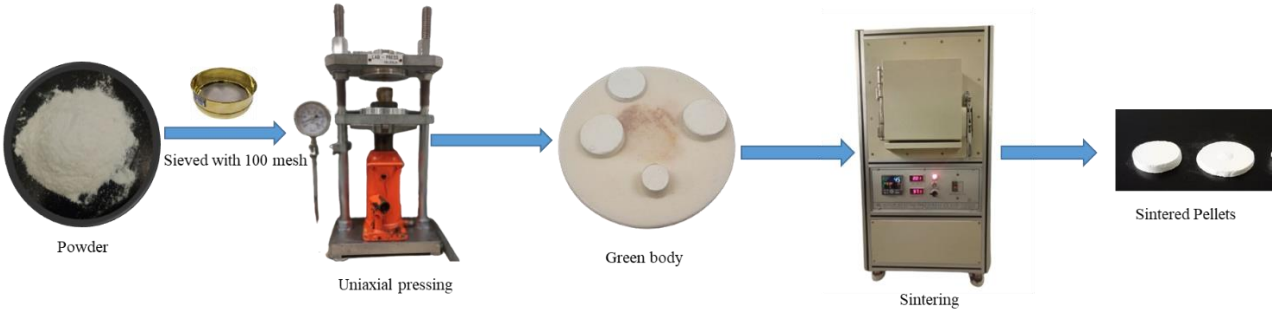

Figure 3. 3: Fabrication of mullite ceramics

2.12 Characterization

The dried gels were characterized using differential thermal analysis (TGA/DTA). TGA/DTA of mullite precursors were performed on thermos analyzer Netzsch Model 409 under the constant synthetic air flow of 50 cm^3 min^{-1}, at the heating rate of 15 ^0C min^{-1}. X-ray diffraction analysis was done using Shimadzu XRD -7000 diffractometer. Diffraction patterns was determined with Cu Kα (λ=1.54056 Å) at a scanning rate of 40/min over 2θ of 10 to 80. The measurement condition also runs with a voltage of 40kv, and 30mA. Field Emission Scanning electron microscopy (FESEM, CZ/MIRA I LMH/HS) was used to observe the surface structure of sintered body, and Energy Dispersive Spectroscopy (EDS) used to identify and quantify the elements present in a sample. Fourier Transform Infrared Spectroscopy (FTIR) with Spectrum (NicoletTMiS50). It was performed using KBr pellets for the chemical functional group analysis.

2.13 Physical properties test

The ASTM standard C 373-88 (1999) provides guidelines for determining the water absorption, bulk density, and apparent porosity of fired unglazed white-ware products. To begin, the dried weight of the sample was measured and recorded. Next, a water bath was filled with distilled water and the sintered mullite sample was carefully placed within it. The system was then placed on a heater for boiling, which was maintained for 4 hours. During this period, the sample was completely submerged in water and was not allowed to come into contact with the heated bottom of the container. If the water level decreased, more water could be added. After the boiling period, the sample was cooled to room temperature, covered with water, and stored in water for 24 hours before being weighed. The suspended weight of the sample was then measured and recorded. This was achieved by suspending the sample in a wire loop in water and attaching the other end to a balance. Finally, the saturated weight (soaked weight) was measured after removing all visible water droplets from the surface of the sample using a wet cloth or moistened, lint-free linen or cotton cloth. The sample was then weighed using a balance and the weight recorded. It is important to perform weight measurements immediately to avoid errors.

$$\text{Water Absorption} = [(M - D)/D] \times 100 \quad \ldots\ldots\ldots\ldots\ldots \quad 3.1$$

$$\text{Bulk density} = D/(M - S) \quad \ldots\ldots\ldots\ldots\ldots\ldots \quad 3.2$$

$$\text{Apparent porosity} = (M - D)/(M - S)] \times 100 \quad \ldots\ldots\ldots\ldots\ldots \quad 3.3$$

Where, M = Soaked weight, S = Suspended weight, D = Dry weight

Linear shrinkage in ceramics refers to the reduction in size of a ceramic body as it undergoes drying and firing processes. This dimensional change is typically measured along a single axis and is a critical factor in the manufacturing and design of ceramic products, as it can affect the final size and shape of the piece (Tiffo et al., 2015b).

$LS=L_2-L_1/L_1$…… 3.4

Where L_1 = dimension of green body, L_2 = dimension of sintered body

2.14 Mechanical test

Samples were tested in accordance with the standard ASTM C773-88 at the Adama Science and Technology University in the mechanical engineering laboratory using a universal testing machine. The test specimens were right cylinders with dimensions of either 11.6 mm in diameter, depending on their capacity level (for 10KN load the preferred sample size which have estimated compression strength above 375). Prior to testing, the samples were cleaned. Then the samples were carefully centered in the machine between the contact blocks, and the load was applied continuously and without impact shock until ultimate failure.

2.15 Dielectric strength

Dielectric strength for insulator samples was computed by measuring their breakdown voltage using a high voltage testing machine (model TERCO HV 1103), found at Addis Ababa University, department of electrical engineering. Dielectric strength is measured by applying a voltage to a material until breakdown occurs, which is the point at which the material can no longer resist the electrical stress and becomes electrically conductive (Appelhans, 2013). The dielectric breakdown strength is typically expressed in terms of voltage per unit thickness (kV/mm) and is determined by the voltage at which a material fails electrically.

Dielectric strength = break down voltage (kV)/the thickness of the sample (mm)…… 3.5

CHAPTER 3

RESULTS AND DISCUSSION

3.1 Results of Extracted Silica

3.1.1 XRD Results analysis

Figure 4.1 presents x-ray diffraction (XRD) patterns of pure silica phase formation. The only observed major peak observed at $2\theta=22.5^0$, corresponding to the silica matrix and indicate its amorphous structure. The absence of sharp peak at room temperature indicates the absence of crystallinity and the absence of any crystalline impurity (Dhaneswara et al., 2020; Vaibhav et al., 2015; Yuvakkumar et al., 2014)

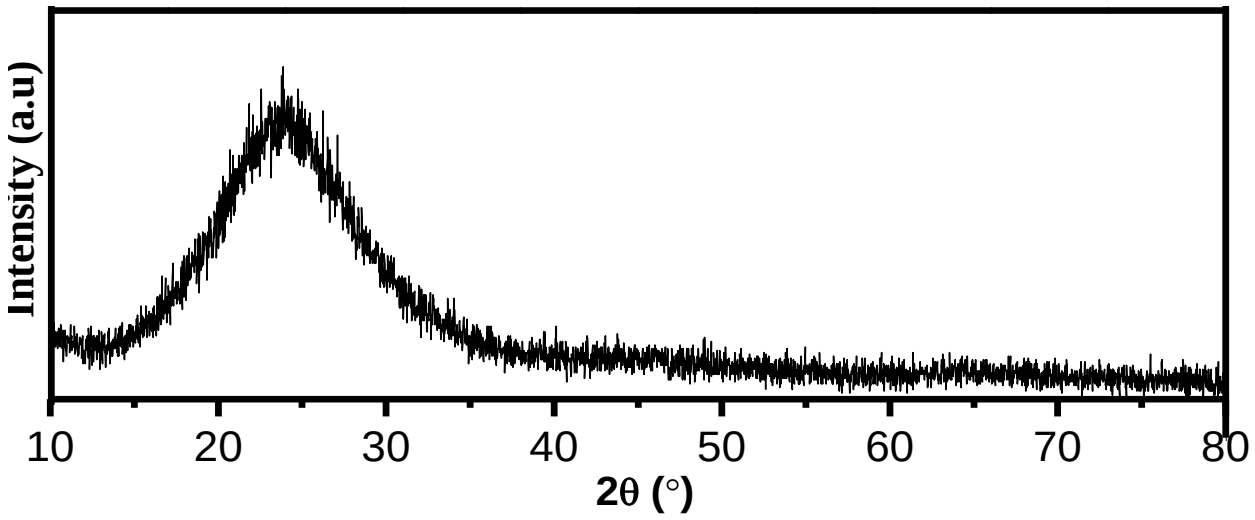

Figure 4. 1: XRD pattern of extracted silica

3.1.2 FTIR Analysis

Figure 4.2 shows results of the FTIR spectra of silica. The formation of silica structure was demonstrated by bands of Si-O symmetrical elongation vibration observed at 796 cm^{-1} and 445 cm^{-1} . At 940 cm^{-1} vibration mode of Si-O is revealed by a weak absorbance band (Dhaneswara et al., 2020). Additionally, the asymmetric elongation of the siloxane framework, Si-O-Si vibration, was at around 1057 cm^{-1}. Whereas the peak at 3340 cm^{-1} more likely to be related to Si-OH

stretching mode in silica, instead of H-OH in water or both, and the peak at 1635cm^{-1} is assigned to H-O-H bending vibration (Vaibhav et al., 2015; Yuvakkumar et al., 2014).

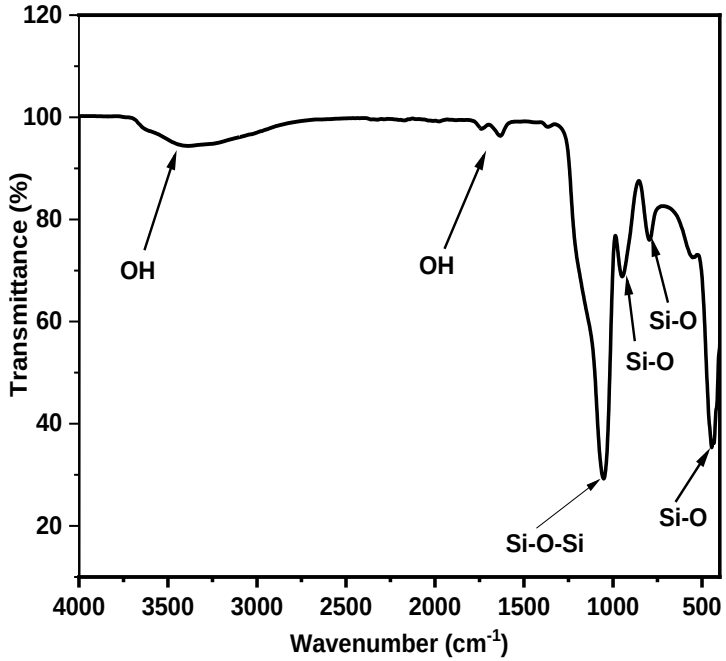

Figure 4. 2: FTIR spectra of extracted silica

3.2 Analysis of Synthesized Aluminosilicate Gels

3.2.1 XRD Analysis

Figure 4.3 shows the XRD patterns of the calcined mullite precursors after being heated for 2hrs at a rate of 10 ^{0}C/min to 1350 ^{0}C. An alpha alumina (Al_2O_3) and cristobalite SiO_2 phases exist in the MC1 and MC2 respectively. XRD results of the MC 3 show coexistence of mullite and cristobalite phases, indicating that there is excess amount of silica gel precursors than that of the optimum concentration. It would be presumed that excess silica gel were present in free state, then during continued heating above 1200 C the amorphous silica transforms to cristobalite and appear at peaks of 2θ value of 21.8^0 (Lee et al., 2002). On the other hand, since the silica gel precursor is below optimum condition, aluminosilicate gels contain excess aluminium hydroxide. Therefore, up on heating above 1150 ^{0}C aluminium hydroxide which found in free state transform to alumina (PDF Card No.# 00-046-1212) peak at 2θ value of 26.67^0, 37.78^0, 43.25^0, 52.47^0,57.55^0 and 68.35^0. MC 2 composition shows the single phase mullite (PDF Card No.# 00-015-0776). The crystallization of mullite without the individual crystallization of α-A1203 and/or cristobalite

indicates that the mixing method employed provided a very good degree of mixing between boehmite and silica particles.

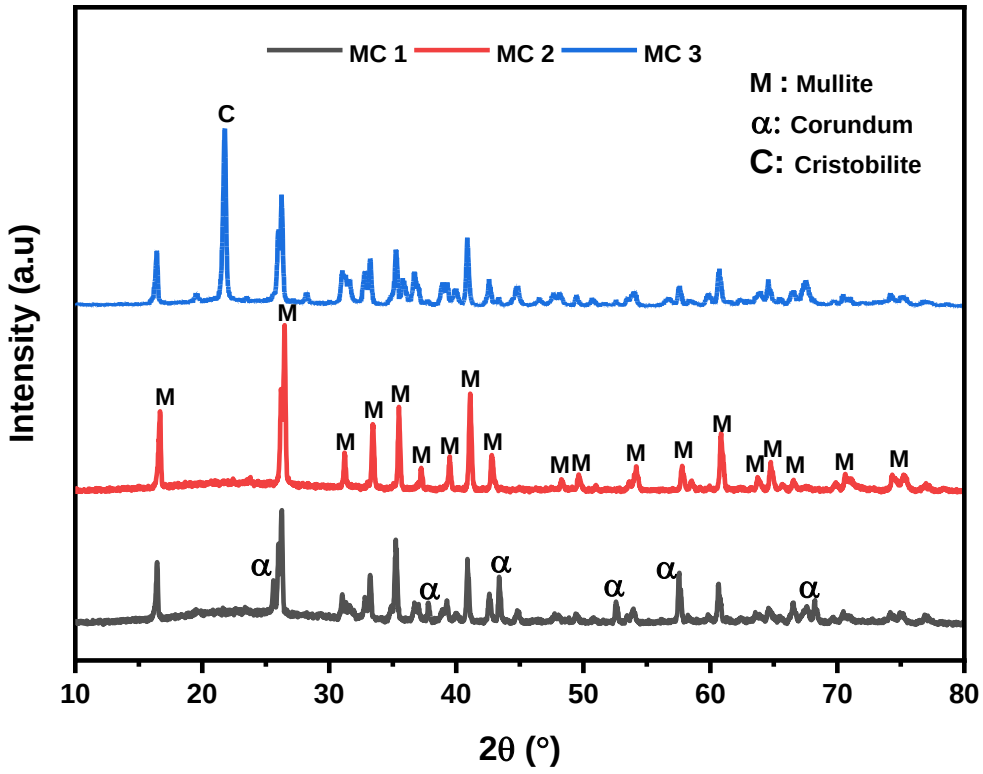

Figure 4. 3: XRD pattern of sintered aluminosilicate gel at 1350 ^{0}C for 2hrs

Batch Mark	Amount of ANN taken (Molar)	Amount of silica gel taken (ml)
MC 1	0.34	23
MC 2	0.34	30
MC 3	0.34	37

Table 4. 1: Batch composition of ANN and synthesized silica gel

3.2.2 Thermo-Gravimetric Analysis (TGA)

Figure 4.4 shows TG-DTA curves of the MC 2 sample heated from 25◦C to 1300 ◦C at 15 ◦C/min. The DTA curve revealed the existence of an endothermic peak and two exothermic peaks. The

endothermic peak between 25^0C and 650^0C is due to water evaporation, the condensation of the surface silanol groups and the dehydration of pseudo-boehmite (WEI & Halloran, 1988a). Due to the intrinsic presence of crystal water, gels or powders that are prepared by using boehmite undergo large weight losses due to the decomposition of boehmite above 400°C (Kara & Little, 1996). The TG curve showed a mass loss of around 33wt%, in the temperature range 25^0 C–650^0C. The first exothermic peak at about 970^0C is related to the formation of the spinel. Above 970^0C the mass gain occurred due to the transformation of dehydrated substances into spinel and crystallization of mullite (Lamara et al., 2022). The second exothermic peak at 1147◦C results from the crystallization of mullite. Thus, mullization temperature is indicated by an exothermic at 1147 ^{0}C; which is in accordance with the earlier report from the sol gel drived mullite (Keziz, Heraiz, et al., 2023).

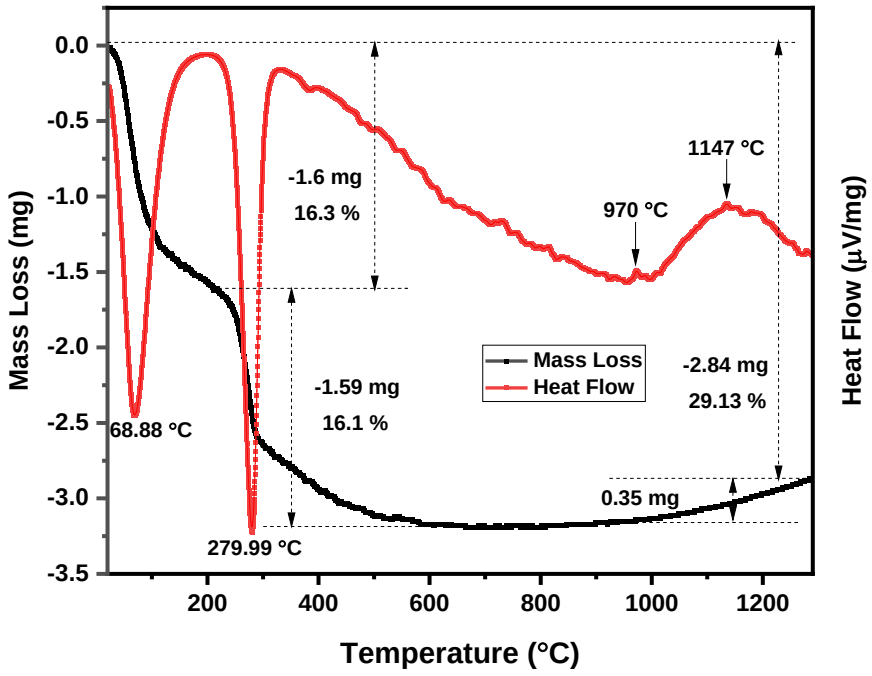

Figure 4. 4: TGA/DTA curve of the aluminosilicate gels powder

3.3 Mullite Formation

3.3.1 XRD Analysis

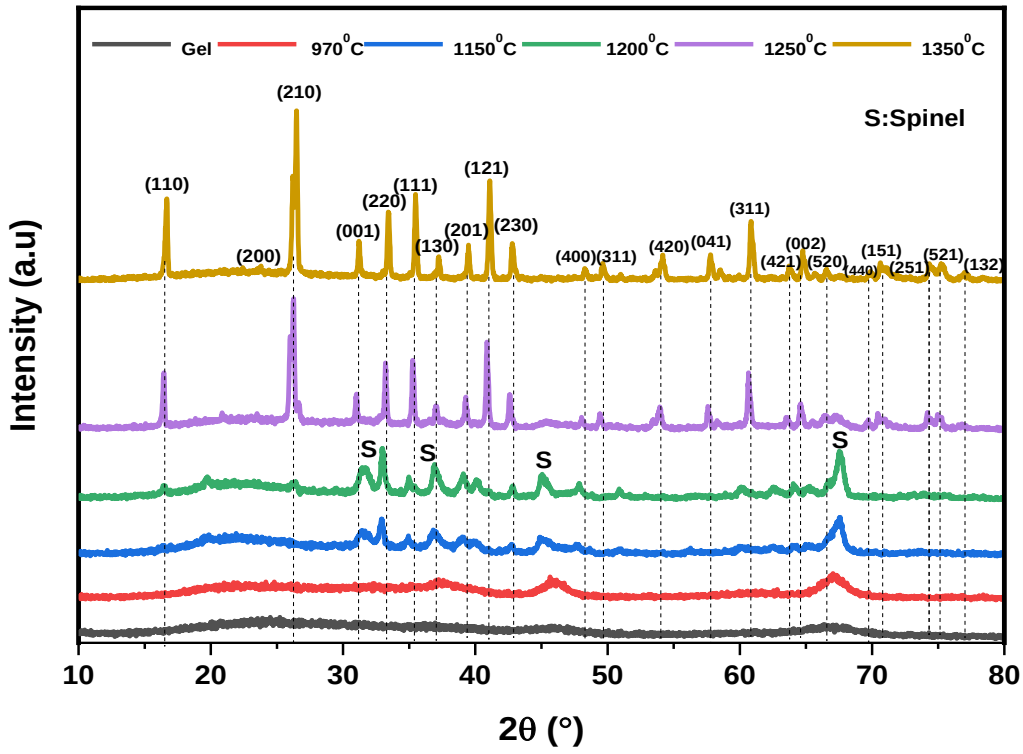

Figure 4. 5: XRD pattern of firing aluminosilic gel for different temperature

Figure 4.4 illustrates the XRD pattern of 25°C, 970°C, 1150°C, 1200°C, 1250°C and 1350°C sintered aluminosilicate gels formed from 30ml of silica gel and 0.34M of aluminum nitrate solution. It can be clearly noticed that aluminosilicate gels is amorphous before calcination. This is due to both precursors of silica and alumina found as amorphous below their phase transformation temperature 1200 ^{0}C and 1150 ^{0}C, respectively (WEI & Halloran, 1988a). But, upon heating the powders started to crystallize at 970 ^{0}C with the formation of spinel. These are due to incorporation of some silica in γ-Al2O3 phase forming Al–Si spinel at 970^{0}C prior to mullite formation process (Das, 2003). And the spinel phase could exist until 1200 ^{0}C. Then this spinel phase undergoes a slow transformation into orthorhombic (stable) mullite as temperature increases to 1250 ^{0}C. This is due to spinel converted into mullite through the diffusion-reaction from activated alumina to the silica or by a gradual decrease in alumina content within the mullite solid solution (Li & Thomson, 1991).

However, upon heating until 1350^{0}C the crystal growth continued and can influence the size and refinement of crystals in a system, which could be extrapolated to the behavior of mullite (Eskin, 2000).

The mullite formation mechanism in the system of silica gels and aluminum nitrate solution is schematically represented in Figure 4.6. A silica gel is a two phase system, a liquid and solid one both continuous as fig (4.5). The solid phase results from the gellification of a sol (Bisson et al., 2003). And aluminum solution is found as aluminum free ions at atomic levels after hydrolysis. However, during gelation these aluminum ions transformed to activated alumina and surround the silica gel, and causes them to unite in a continuous network, forming the gel that is homogeneous and reactive (L. K. S. Lima et al., 2022). Therefore, the number of diffusion sites for activated alumina into silica is increased due to the high surface area of silica and the shorter diffusion distance. It is attributed to the mullitization at low temperature, i.e., 1150 °C and above by the viscous flow (Kara & Little, 1996). And this idea have been proved by many researcher who works with different precursors (Das, 2003)

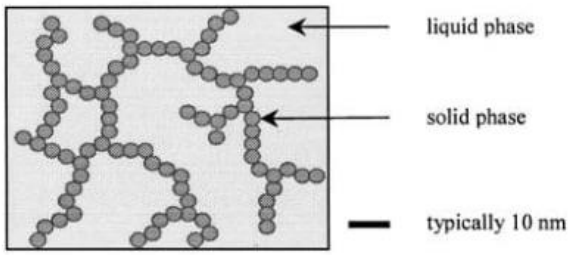

Figure 4. 6: Schematic structure of the solid phase of a silica gel (Bisson et al., 2003)

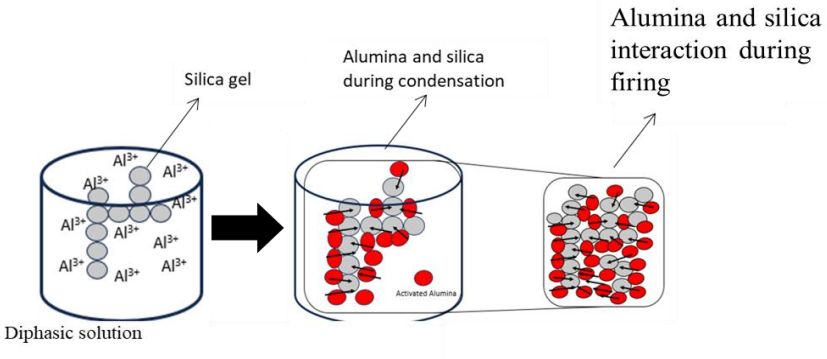

Figure 4. 7: Schematic representation of mullite formation reaction mechanism with reactive alumina and gels containing silica.

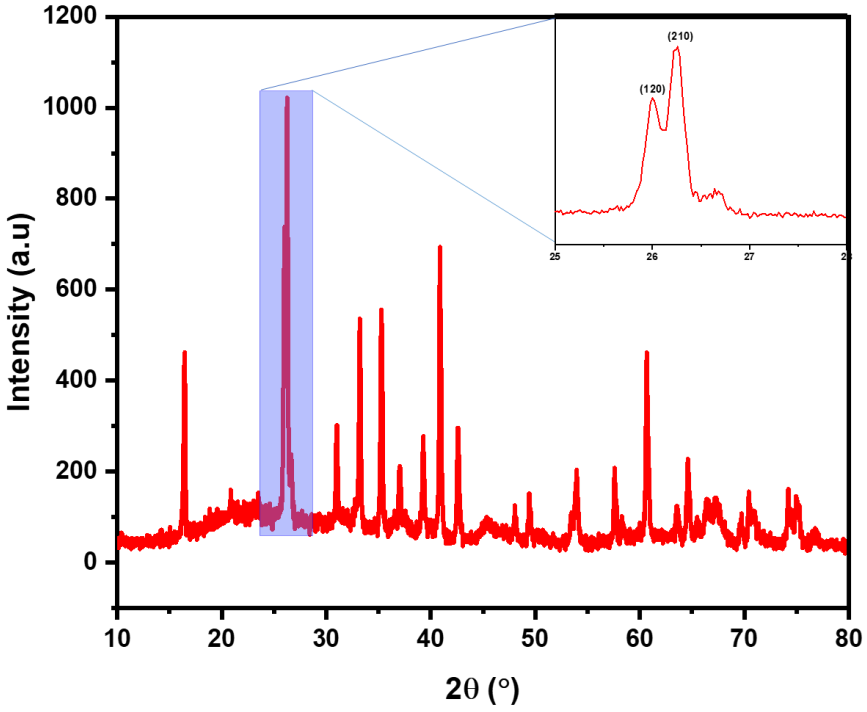

Figure 4. 8: XRD pattern of sintered aluminosilicate gel at 1350^{0}C for 2hrs

Figure 4.7 demonstrates the orthorhombic mullite can be differentiated most readily from the tetragonal mullite by observing the division of the single diffraction peak of 120 and 210, which is also the predominant diffraction peak. Moreover, the mullite initially forms in the orthorhombic structure, as evidenced by the separation of the 120 and 210 peaks (Li & Thomson, 1991). In the case of 120 and 210 peaks overlapped it showed the phases of pseudotetragonal (Johnson et al., 2001)

3.3.2 Fourier Transform Infrared Spectroscopy (FT-IR) Analysis

The composition and bonding status of functional groups are examined by Fourier transform infrared spectroscopy (FTIR) analysis.

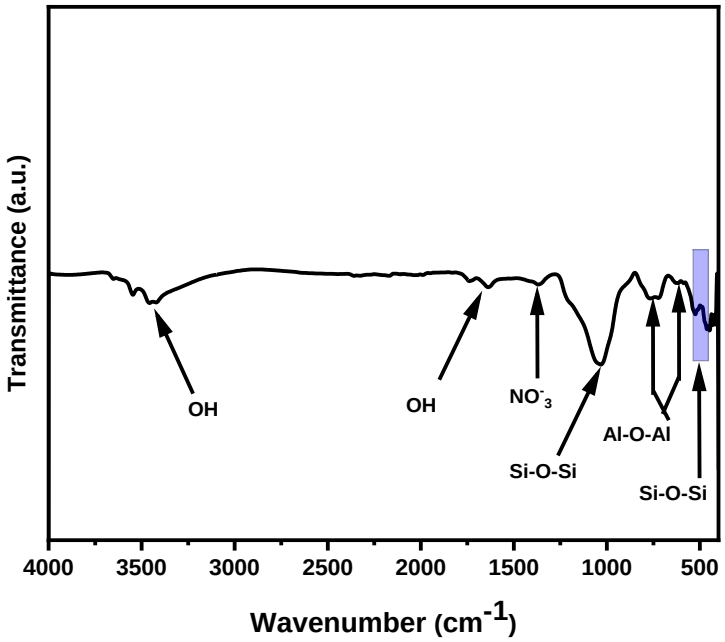

Figure 4. 9: FTIR spectra of aluminosilicate gels powder

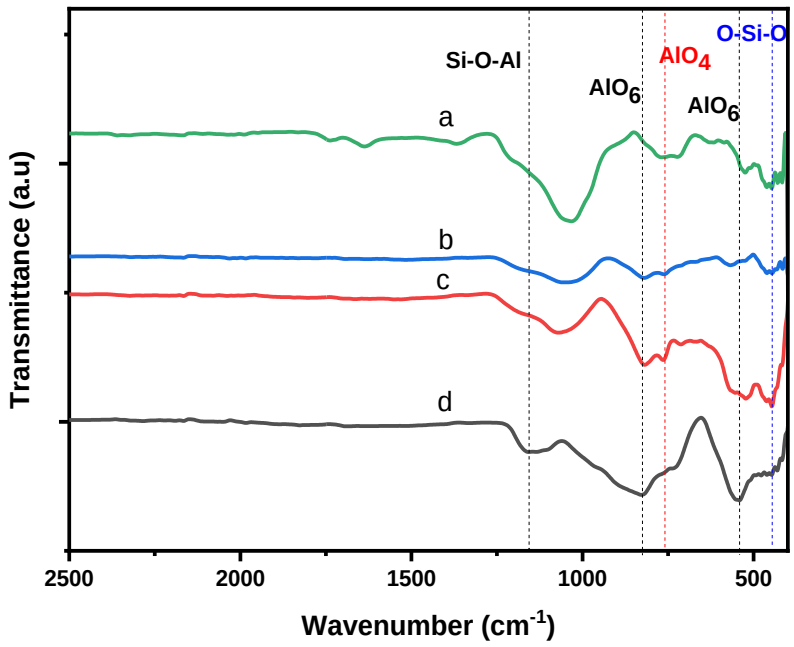

Figure 4. 10: FTIR spectra of sintered aluminosilicate gel powder a) 25^0C, b) 1150^0C, c) 1250^0C and d) 1350^0C

Figure 4.9 indicate the FTIR spectrum of aluminosilicate gels and mullite ceramics. For dried gel, the peaks at 3483 cm^{-1} and the one at 1633 cm^{-1} are assigned, respectively, to the stretching and

bending modes of adsorbed water since the precursor gel is prepared under basic condition (P Padmaja et al., 2001). No characteristic peak corresponding to Al-O-Si linkage was observed in the FTIR spectra of the dried gel, which means both the aluminum hydroxide, $Al(OH)_3$ and silicon hydroxide, $Si(OH)_4$ formed under alkaline conditions precipitated simultaneously. So the precursor gel was diphasic in nature (Roy & Maitra, 2014). The peaks 557 and 470 cm^{-1} were corresponded to the Si-O-Si groups in SiO_2 (Zhang et al., 2009). The peaks located in 1040 cm^{-1} were assigned to bending modes of Si-O-Si (Okada & ŌTSUKA, 1986). Given that the starting material was $Al(NO_3)_3$, and the peak at 1388 cm^{-1} was attributed to the stretching of the entrapped nitrate ions within the gel structure (JAGANNATH et al., 2011)

Upon heating at temperatures from 25-1150°C, a significant change in the spectra was observed in the form of a peak shift from 787 cm^{-1} to 803-806 cm^{-1}. This shift was attributed to the symmetric stretching vibration of Si-O-Al linkages, which suggested the initiation of Al-Si spinel formation within gel structure, and the broad shoulder indicating an extensive formation of Al-Si spinel (JAGANNATH et al., 2011).

Figure 4.10 shows the FT-IR spectra of samples sintered at temperatures 1150 ^{0}C, 1250 ^{0}C, and 1350 ^{0}C for 2hrs in wave number region 400–4000 cm^{-1}. The shoulder appeared on 1040 cm^{-1} of the 1150^{0}C and 1250^{0}C spectrum develops into a well assignment broad bands which frequencies of stoichiometry defined band with components at 1163 cm^{-1} at 1350 ^{0}C. These are revealed, respectively, to the asymmetric stretching difference in the spectra of the gel and gel calcined at vibrations of Si–O–Si and Si–O–Al networks (P. Padmaja et al., 2001). Additionally for the orthorhombic (stable) mullite, the FT-IR band at 1,130 cm^1 is less intense than the band at 1,170 cm^{-1} (Campos et al., 2012; Cividanes et al., 2010). With increasing sintering temperature, the absorption intensity of the peaks attributable to the Al–O bond vibration at 830 cm^{-1} (AlO_4), 740 cm^{-1} (AlO_4), and 570 cm^{-1} (AlO_6) gradually increased (Lee et al., 2004). Increased in AlO_6 suggest a disordered distribution of octahedral sites (Li & Thomson, 1990). And weak band at 460 cm^{-1} correspond to the O-Si-O (Cividanes et al., 2010). Based on the FTIR data, it was observed that as the sintering temperature was increased up to 1350 ^{0}C, the aluminosilicate gels transformed into crystalline mullite with both tetrahedral and octahedral coordination of Al^{3+} ions (Komarneni & Rutiser, 1996; Zhao et al., 2002).

3.3.3 Scanning Electron Microscope (SEM) and EDS Analysis

The mullite formation mechanism, in the case of diphasic precursors it has been found that the growth rate of the mullite grains is controlled by dissolution of the alumina particles into the amorphous silica-rich phase (Sales & Alarcón, 1996). Figure **a** exhibit interaction between silica core and alumina layer in precipitation stage. However, during the sintering around $115O^0C$, the Si-O-Al linkage could be formed in this interface. Thus, the mullite crystallization could be evolved more easily. The mullite crystallization showed above 1250^0C with the shapes of rod and flakes (fig **b**), and equiaxed to elongated mullite grain structures was found within a narrow range of composition which is agree with the nominal Al/Si ratio of 3/1 (Table 4.2). Figure **c** showed upon heating until 1350^0C the crystal growth continued and can influence the size and refinement of crystals in a system.

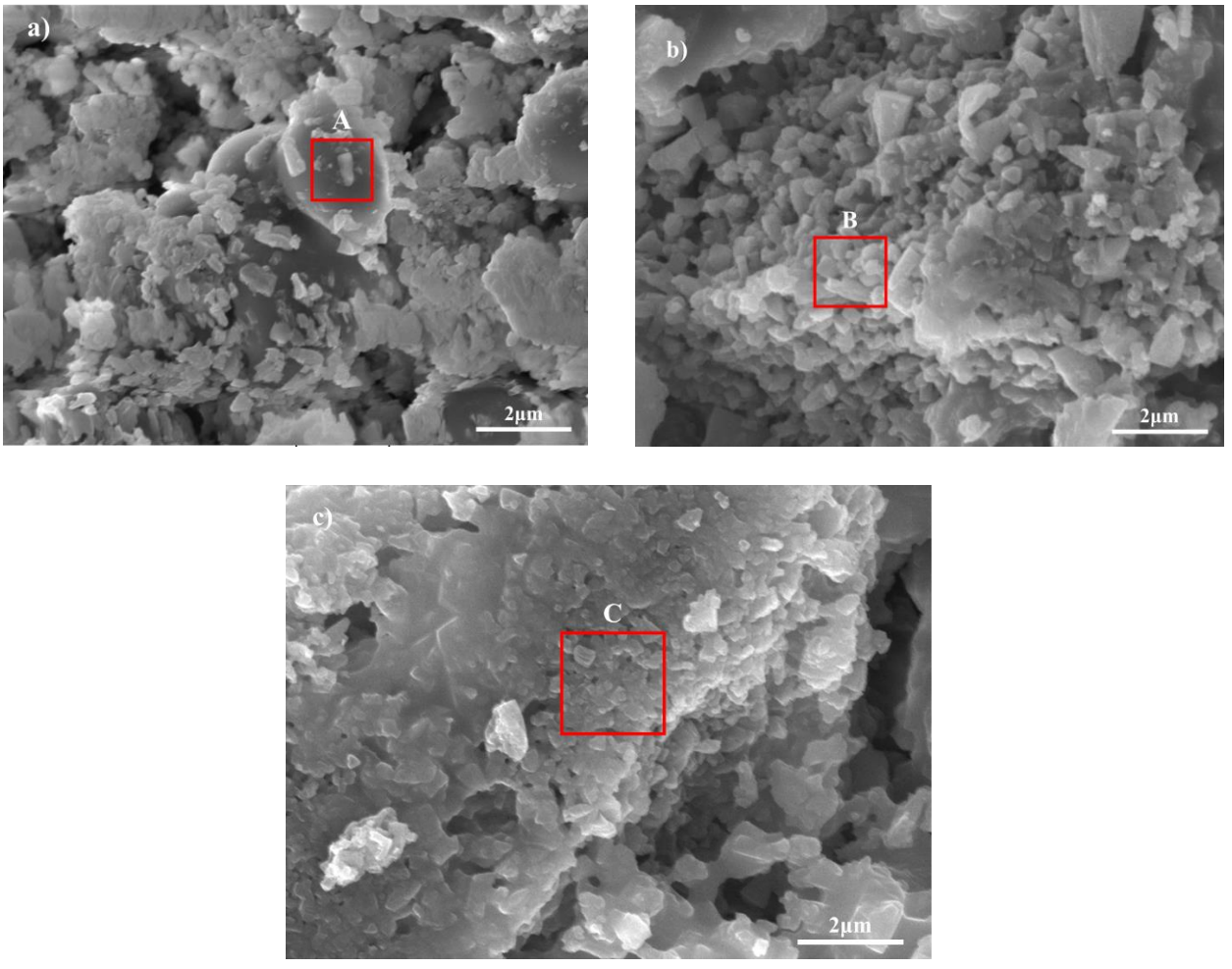

Figure 4. 11: SEM images of mullite samples with different sintering temperature: a) 1150^{0}C (b) 1250^{0}C (c) 1350^{0}C

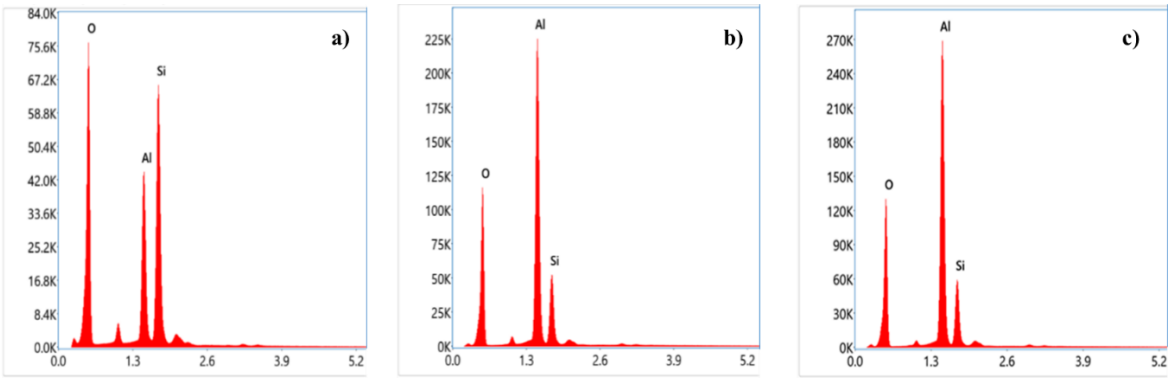

Figure 4. 12: EDS analysis of sintered mullite a) 1150^{0}C (region A) b) 1250^{0}C (region B), and c)1350^{0}C (region C)

Element	**Region C (Weight %)**	**Nominal mullite composition (weight %) (Schmidt et al., 2019)**
O	49.9	61.9
Al	38.3	28.6
Si	11.8	9.5
Ratio Si/Al	0.308	0.332
Ratio Al/Si	3.24	3.01

Table 4. 2: Elemental analysis of spots located in the region C and nominal mullite composition

From the phase diagram of alumina-silica system, it is stated that single phase mullite solid solution range consists of (71.8–74.3) wt% of alumina and (28.2–25.7) wt% of silica (Deng et al., 2018). For this present work, mullite ceramic synthesized here, was gives 0.308 Si/Al ratio, whereas the nominal mullite ceramics composition gives 0.332 Si/Al ratio. According to previous studies mullite's composition is found in stable region of solid solutions (70.5 to 74.0 wt% of alumina, or Al/Si from 2.8/1 to 3.3/1) (Deng et al., 2018; Schmidt et al., 2019). In this work Al/Si values of synthesized mullite is 3.24, so the required valued are met and confirmed its formation in a given stable mullite range.

3.4 Physical and Mechanical Properties, and Dielectric Strength of Fabricated Ceramics

3.4.1 Physical Properties

The water absorption of the fired bodies is depicted in Figure 4.13(a). This measurement serves as an indicator of the porosity of the fired body. It was observed that the sintered aluminosilicate gel at 1150 exhibited a higher water absorption of approximately 8.26%, due to its 18.95% porosity, which allowed water to penetrate the body. As the sintering temperature increases, the pores within the material tend to close, reducing porosity and the capacity for water absorption. The presence of porosity was further confirmed by the SEM images presented in Figure 4.11(a). Figure 4.11(c) illustrates that as the sintering temperature rises from 1150°C to 1350°C, the material undergoes densification due to the growth of grains and the elimination of pores, resulting in a decrease in porosity to 0.81% and a corresponding reduction in water absorption to 0.89%. Additionally, Figure 4.13(c) demonstrates that at a sintering temperature of 1350°C, a significant densification occurs, resulting in a ceramic with a density of 2.71 g/cm³. The density of ceramics typically increases with an increase in sintering temperature due to the diffusion of particles, which allows them to move and fill, leading to a decrease in overall volume and an increase in density (He et al., 2018; Wang et al., 2024). This decrease in volume is referred to as linear shrinkage. Figure 4.13(d) illustrates the shrinkage percentages at temperatures of 1150°C, 1250°C, and 1350°C, resulting in 12%, 17%, and 18.5%, respectively. This indicates that during heating, while densification occurs and pores are removed, particles are rearranged.

Generally, at 1350 ^{0}C synthesized mullite, showed 0.89% water absorption, 0.8% porosity, 3.02 g/cm³ density, and 18.2% shrinkage. High density and low porosity contain mullite ceramics exhibit higher dielectric strength compared to their porous counterparts due to the lack of voids and discontinuities that can serve as pathways for electrical breakdown (Xia et al., 2022). The presence of pores in mullite ceramics can interrupt the uniformity of the material, creating points of weakness where electrical breakdown can initiate more easily. This is because air or other gases trapped within the pores have lower dielectric strength than the solid ceramic matrix (Zhang et al., 2020; T. Zhang et al., 2019).

Table 4. 3: Physical properties sintered mullite ceramics at different temperature

Samples	Sintered temperature (^{0}C)	Water absorption (%)	Porosity (%)	Density (g/cm^3)	Linear Shrinkage (%)
Sample 1	1150	8.26	18.95	2.29	12
Sample 2	1250	1.69	4.7	2.71	16
Sample 3	1350	0.89	0.81	3.02	18.5

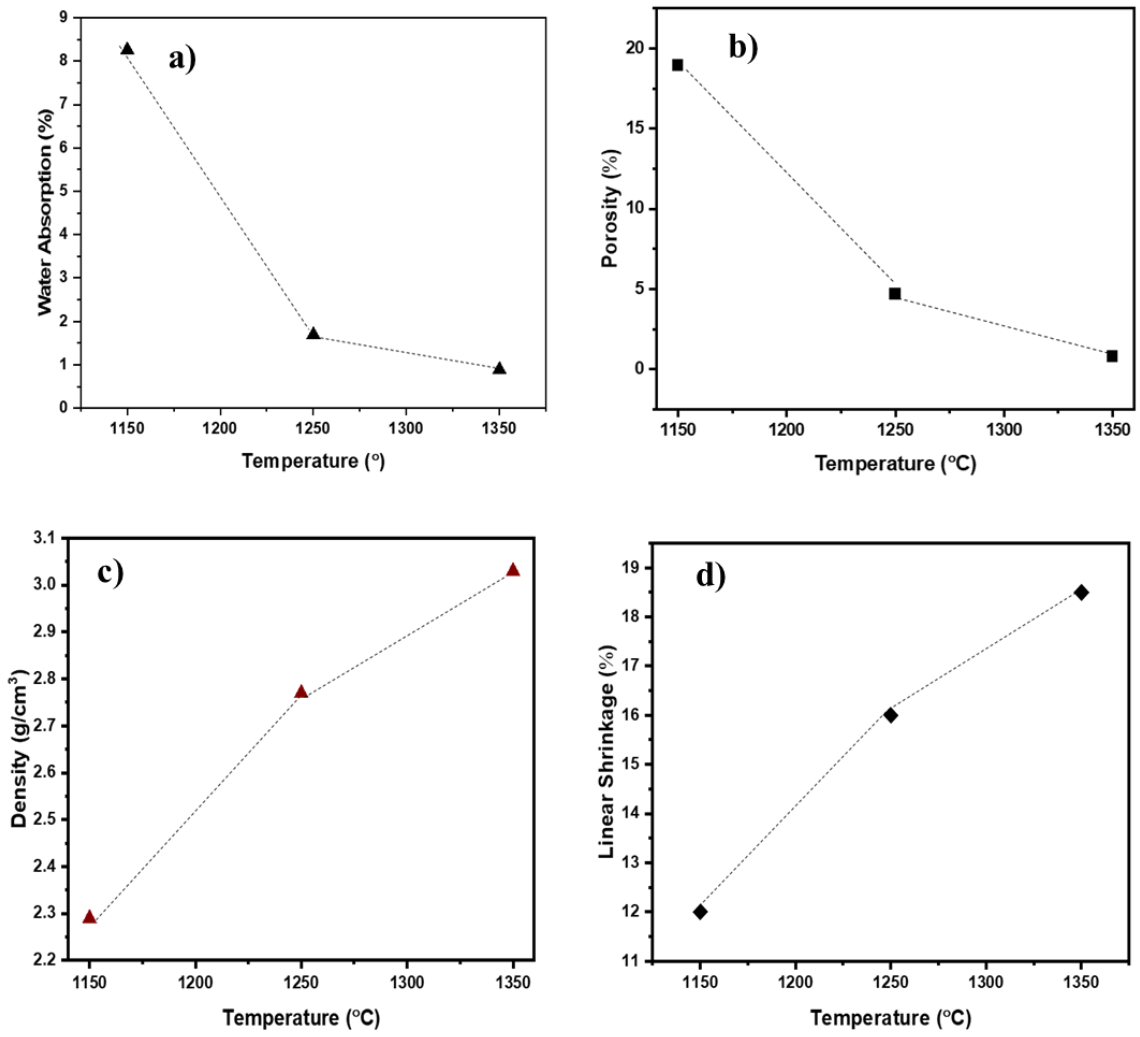

Figure 4. 13: : (a) Water absorption, (b) Porosity, (c) Density and (d) linear shrinkage of sintered mullite ceramics at different temperature

3.4.2 Compression Strength

The compressive strength of mullite ceramics increases with the rise in sintering temperature Figure 4.14, reaching a maximum value of 420 MPa at 1350°C after 2hrs duration. This enhancement in strength is primarily due to the densification of the ceramic material, which occurs as the temperature increases. During the densification process, pores within the ceramic body are eliminated, and potential crack initiators are removed (Callister Jr & Rethwisch, 2020). This reduction in porosity and the elimination of structural flaws contribute significantly to the overall strength and durability of the mullite ceramics.

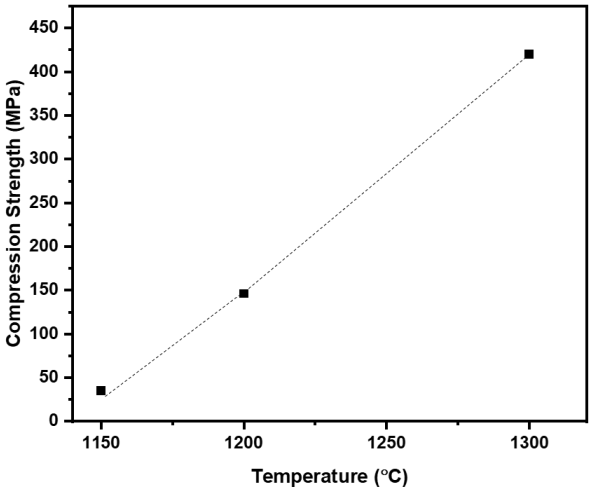

Sintering temperature (^{0}C)	Compression Strength (MPa)
1150	35
1250	146
1350	420

Table 4. 4: Mechanical strength of sintered mullite ceramics at different temperature

Figure 4. 14 : *Compression strength of sintered mullite ceramics at different temperature*

3.4.3 Dielectric Strength

The dielectric strength values for the mullite ceramics sample, as determined at different sintering temperatures of 1150°C, 1250°C, and 1350°C for a duration of 2 hours, are portrayed in Figures 4.15. It is evident that the dielectric strength displayed an upward trend as the temperature increased, with the highest value of 10.2 KV/mm achieved at 1350°C. According to the research conducted by Roy et al. (2021), mullite ceramics with a dielectric strength of 9.8 KV/mm and above are employed as electrical insulators at room temperature, making them suitable for use in electronic devices (Roy et al., 2021). Furthermore, these results meet the ASTM standard for electronic applications. The rise in dielectric strength with increasing sintering temperature can be attributed to several factors. As sintering temperature rises, the material typically undergoes densification, which leads to a decrease in porosity and the elimination of voids that can act as

sites for electrical breakdown (Al-Hilli & Al-Rasoul, 2010). Additionally, as the temperature increases, the conversion of mullite phases progresses, and eventually, complete conversion to mullite phases occurs. Consequently, since the dielectric strength depends on mullite phases, it exhibits improved properties at 1350°C.

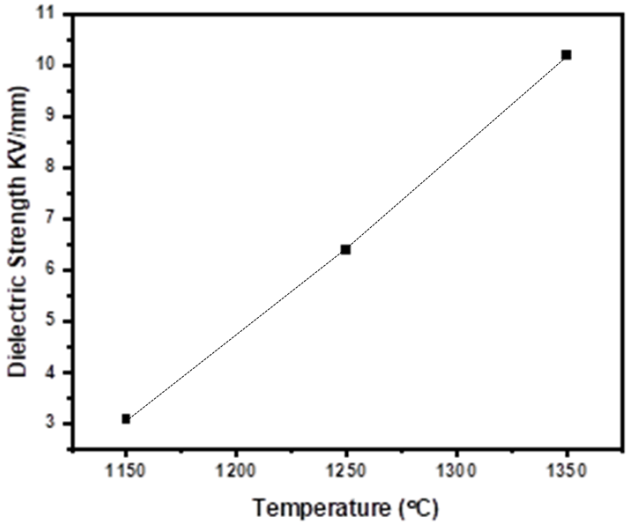

Figure 4. 15: *Dielectric strength of sintered mullite ceramics at different temperature*

Sintering temperature (^{0}C)	Dielectric Strength (KV/mm)
1150	3
1250	6.4
1350	10.2

Table 4. 5: Dielectric strength sintered mullite ceramics *at different temperature*

CHAPTER 4

CONCLUSIONS AND RECOMMENDATION

4.1 Conclusions

Pure silica was successfully synthesized from filter cake waste using sol gel methods. Therefore, extracted silica achieved requirement of silica that needed for mullite ceramics. Then, aluminosilicate gels was synthesized by using diphasic gels methods. XRD and FT-IR results confirmed the formation of aluminosilicate gels by showing amorphous phases at lower temperature and the absence of Al-O-Si linkage in the spectra of the dried gel, respectively.

Dried precursor was transformed into Al-Si spinel immediately after the crystallization at 970^0C, then a trace of crystalline mullite was produced at 1150^0C. Consequently, the single phase of mullite was obtained by sintering of the precursors at temperatures higher than 1250^0C, and the peak of the XRD and FTIR were sharpened with increasing temperature, and it forms rod like morphology. Finally, the temperature above 1350^0C the samples show densification and crystal growth.

The electrical performance of synthesized mullite was evaluated at various temperatures of 1150°C, 1250°C, and 1350°C for a constant duration of 2 hours, resulting in 3 kV/mm, 6.6 kV/mm, and 10.2 kV/mm, respectively. According to ASTM standards, the mullite ceramics synthesized exhibited excellent electrical properties, with the highest value of 10.2 kV/mm achieved through densification at 1350°C for 2 hours, as confirmed by SEM results. The physical properties of the synthesized mullite, including 0.89% water absorption, 0.81% porosity, 3.02 g/cm³ density, and 18.2% shrinkage, as well as a compression strength of 420 MPa, collectively suggest that it is suitable for dielectric applications. The densification process was further confirmed by the physical properties of the synthesized mullite.

5.2 Recommendation

1. Optimization of ceramic fabrication based on particle size, sintering time and compaction worked the performance should be updated.

2. Conduct AC impendences spectroscopy test to assess the dielectric constant, dielectric loss and AC conductivity.

REFERENCE

9 - Silicon. (1997). In N. N. Greenwood & A. Earnshaw (Eds.), *Chemistry of the Elements (Second Edition)* (pp. 328-366). Butterworth-Heinemann. https://doi.org/https://doi.org/10.1016/B978-0-7506-3365-9.50015-8

Aksay, I. A., Dabbs, D. M., & Sarikaya, M. (1991). Mullite for structural, electronic, and optical applications. *Journal of the American Ceramic Society*, *74*(10), 2343-2358.

Al-Hilli, M. F., & Al-Rasoul, K. T. (2010). Influence of glass addition and sintering temperature on the structure, mechanical properties and dielectric strength of high-voltage insulators. *Materials & Design*, *31*(8), 3885-3890. https://doi.org/https://doi.org/10.1016/j.matdes.2010.02.048

Anggono, J. (2005). Mullite ceramics: its properties structure and synthesis. *Jurnal Teknik Mesin*, *7*(1), 1-10.

Appelhans, L. (2013). *Humidity effects on wire insulation breakdown strength*.

Aripin, H., Mitsudo, S., Prima, E., Sudiana, I., Kikuchi, H., Sano, S., & Sabchevski, S. (2015). Crystalline mullite formation from mixtures of alumina and a novel material—Silica xerogel converted from sago waste ash. *Ceramics International*, *41*(5), 6488-6497.

Avnir, D., Levy, D., & Reisfeld, R. (1984). The nature of the silica cage as reflected by spectral changes and enhanced photostability of trapped rhodamine 6G. *The Journal of Physical Chemistry*, *88*(24), 5956-5959.

Belmonte, M. (2006). Advanced ceramic materials for high temperature applications. *Advanced engineering materials*, *8*(8), 693-703.

Bereda, Y. B., Tesfamariam, B. B., Desissa, T. D., Habtamu, G., Singh, B., & Ramulu, P. J. (2023). Utilization of silica-enriched filter cake industry by-products as partial ordinary portland cement replacement. *Materials Research Express*, *10*(2), 025502.

Bisson, A., Rigacci, A., Lecomte, D., Rodier, E., & Achard, P. (2003). Drying of silica gels to obtain aerogels: phenomenology and basic techniques. *Drying technology*, *21*(4), 593-628.

Biswal, B., Mishra, D., Das, S. N., & Bhuyan, S. (2021a). Structural, micro-structural, optical and dielectric behavior of mullite ceramics. *Ceramics International*, *47*(22), 32252-32263.

Biswal, B., Mishra, D. K., Das, S. N., & Bhuyan, S. (2021b). Structural, micro-structural, optical and dielectric behavior of mullite ceramics. *Ceramics International*, *47*(22), 32252-32263. https://doi.org/https://doi.org/10.1016/j.ceramint.2021.08.120

Boccaccini, A., Khalil, T., & Bücker, M. (1999). Activation energy for the mullitization of a diphasic gel obtained from fumed silica and boehmite sol. *Materials Letters*, *38*(2), 116-120.

Bokov, D., Turki Jalil, A., Chupradit, S., Suksatan, W., Javed Ansari, M., Shewael, I. H., Valiev, G. H., & Kianfar, E. (2021). Nanomaterial by sol-gel method: synthesis and application. *Advances in Materials Science and Engineering*, *2021*, 1-21.

Bradt, R. C. (2008). The Sillimanite Minerals: Andalusite, Kyanite, and Sillimanite. In J. F. Shackelford & R. H. Doremus (Eds.), *Ceramic and Glass Materials: Structure, Properties and Processing* (pp. 41-48). Springer US. https://doi.org/10.1007/978-0-387-73362-3_3

Burnham, C. W. (1963). Refinement of the crystal structure of sillimanite. *Zeitschrift für Kristallographie-Crystalline Materials*, *118*(1-6), 127-148.

Callister Jr, W. D., & Rethwisch, D. G. (2020). *Callister's materials science and engineering*. John Wiley & Sons.

Campos, T. M. B., Cividanes, L. S., Brunelli, D. D., Sakane, K. K., & Thim, G. P. (2012). Effect of ethylene glycol on the mullite crystallization. *Journal of the European Ceramic Society*, *32*(4), 835-842. https://doi.org/https://doi.org/10.1016/j.jeurceramsoc.2011.09.028

Cassidy, D., Woolfrey, J., Bartlett, J. R., & Ben-Nissan, B. (1997). The effect of precursor chemistry on the crystallisation and densification of sol-gel derived mullite gels and powders. *Journal of Sol-Gel Science and Technology*, *10*, 19-30.

Catauro, M., & Ciprioti, S. V. (2021). Characterization of Hybrid Materials Prepared by Sol-Gel Method for Biomedical Implementations. A Critical Review. *Materials*, *14*(7), 1788. https://www.mdpi.com/1996-1944/14/7/1788

Chen, L., Wang, Z., Xue, Z., Zhou, G., & Wang, S. (2022). Preparation of mullite ceramics with equiaxial grains from powders synthesized by the sol-gel method. *Ceramics International*, *48*(4), 4754-4762.

Chen, P., Gu, X., Liu, S., Zhu, S., Wang, T., Zhu, Y., Fan, A., & Liu, Y. (2023). Industrial waste silica-alumina gel recycling: Low-temperature synthesis of mullite whiskers for mass production. *Ceramics International*, *49*(6), 9442-9451.

Chen, Z., Li, Z., Li, J., Liu, C., Lao, C., Fu, Y., Liu, C., Li, Y., Wang, P., & He, Y. (2019). 3D printing of ceramics: A review. *Journal of the European Ceramic Society*, *39*(4), 661-687. https://doi.org/https://doi.org/10.1016/j.jeurceramsoc.2018.11.013

Choo, T. F., Mohd Salleh, M. A., Kok, K. Y., & Matori, K. A. (2019). A review on synthesis of mullite ceramics from industrial wastes. *Recycling*, *4*(3), 39.

Ciriminna, R., Fidalgo, A., Pandarus, V., Beland, F., Ilharco, L. M., & Pagliaro, M. (2013). The sol–gel route to advanced silica-based materials and recent applications. *Chemical reviews*, *113*(8), 6592-6620.

Cividanes, L. S., Campos, T. M., Rodrigues, L. A., Brunelli, D. D., & Thim, G. P. (2010). Review of mullite synthesis routes by sol–gel method. *Journal of Sol-Gel Science and Technology*, *55*(1), 111-125.

Cui, K., Zhang, Y., Fu, T., Wang, J., & Zhang, X. (2020). Toughening Mechanism of Mullite Matrix Composites: A Review. *Coatings*, *10*(7), 672. https://www.mdpi.com/2079-6412/10/7/672

da Silva, V. J., da Silva, M. F., Gonçalves, W. P., de Menezes, R. R., de Araújo Neves, G., de Lucena Lira, H., & de Lima Santana, L. N. (2016). Porous mullite blocks with compositions containing kaolin and alumina waste. *Ceramics International*, *42*(14), 15471-15478.

da Silva, V. J., de Almeida, E. P., Gonçalves, W. P., da Nóbrega, R. B., de Araújo Neves, G., de Lucena Lira, H., Menezes, R. R., & de Lima Santana, L. N. (2019). Mineralogical and dielectric properties of mullite and cordierite ceramics produced using wastes. *Ceramics International*, *45*(4), 4692-4699. https://doi.org/https://doi.org/10.1016/j.ceramint.2018.11.161

Das, S. (2003). Al-Si spinel phase formation in diphasic mullite gels. *Ceramics International*, *1*(29), 27-33.

de Sola, E. R., Torres, F. J., & Alarcón, J. (2006). Thermal evolution and structural study of 2: 1 mullite from monophasic gels. *Journal of the European Ceramic Society*, *26*(12), 2279-2284.

Deng, X., Wu, Y., Wei, T., Ran, S., Huang, L., Zhang, H., Li, F., Han, L., Ge, S., & Zhang, S. (2018). Preparation of elongated mullite self-reinforced porous ceramics. *Ceramics International*, *44*(7), 7500-7508. https://doi.org/https://doi.org/10.1016/j.ceramint.2018.01.144

Dhaneswara, D., Fatriansyah, J. F., Situmorang, F. W., & Haqoh, A. N. (2020). Synthesis of amorphous silica from rice husk ash: comparing HCl and CH3COOH acidification methods and various alkaline concentrations. *Synthesis*, *11*(1), 200-208.

Dimitriev, Y., Ivanova, Y., & Iordanova, R. (2008). History of sol-gel science and technology. *Journal of the University of Chemical technology and Metallurgy*, *43*(2), 181-192.

Dislich, H. (1971). New routes to multicomponent oxide glasses. *Angewandte Chemie International Edition in English*, *10*(6), 363-370.

Dislich, H., & Hinz, P. (1982). History and principles of the sol-gel process, and some new multicomponent oxide coatings. *Journal of Non-Crystalline Solids*, *48*(1), 11-16.

Dong, Y., Diwu, J., Feng, X., Feng, X., Liu, X., & Meng, G. (2008). Phase evolution and sintering characteristics of porous mullite ceramics produced from the flyash-Al(OH)3 coating powders. *Journal of Alloys and Compounds*, *460*(1), 651-657. https://doi.org/https://doi.org/10.1016/j.jallcom.2007.06.043

Dong, Y., Feng, X., Feng, X., Ding, Y., Liu, X., & Meng, G. (2008). Preparation of low-cost mullite ceramics from natural bauxite and industrial waste fly ash. *Journal of alloys and Compounds*, *460*(1-2), 599-606.

Duval, D. J., Risbud, S. H., & Shackelford, J. F. (2008). Mullite. In *Ceramic and glass materials: structure, properties and processing* (pp. 27-39). Springer.

Eskin, D. G. (2000). Primary solidification in aluminum alloys under melt overheating. Materials science forum,

Fischer, R. X., Gaede-Köhler, A., Birkenstock, J., & Schneider, H. (2012). Mullite and mullite-type crystal structures. *International Journal of Materials Research*, *103*(4), 402-407.

Fuertes, V., Berges, C., Gallego, A., Enríquez, E., Herranz, G., & Fernández, J. F. (2020). Tailoring dielectric properties of cordierite-mullite ceramics through Ceramic Injection Moulding. *Materials Science and Engineering: B*, *262*, 114783. https://doi.org/https://doi.org/10.1016/j.mseb.2020.114783

Gao, J.-m., Wang, B., Du, Z., Guo, Y., & Cheng, F. (2022). Molten salt synthesis of mullite whiskers entirely derived from fly ash for electronic packaging toughening ceramic applications. *Journal of Materials Research and Technology*, *21*, 3719-3731.

Gao, X., Feng, X., Zhang, D., Zhang, J., Peng, Y., Pan, Z., & Dai, Z. (2023). Synthesis of high-performance mullite ceramics based on associated rare-earth kaolin. *International Journal of Applied Ceramic Technology*, *20*(3), 1535-1546.

Haynes, J. A., Lance, M. J., Cooley, K. M., Ferber, M. K., Lowden, R. A., & Stinton, D. P. (2004). CVD Mullite Coatings in High-Temperature, High-Pressure Air–H2O. *Journal of the American Ceramic Society*, *83*(3), 657-659. https://doi.org/10.1111/j.1151-2916.2000.tb01250.x

He, H., Cai, W., Gao, R., Chen, G., Deng, X., & Fu, C. (2018, 2018//). Effects of Sintering Temperature on Microstructure, Electric Properties of Ba0.7Sr0.3TiO3 Ceramics. Advanced Functional Materials, Singapore.

Hoffman, D., Roy, R., & Komarneni, S. (1984). Diphasic ceramic composites via a sol-gel method. *Materials Letters*, *2*(3), 245-247. https://doi.org/https://doi.org/10.1016/0167-577X(84)90035-1

Hoffman, D. W., ROY, R., & KOMARNENI, S. (1984). Diphasic xerogels, A new class of materials: phases in the system Al2O3-SiO2. *Journal of the American Ceramic Society*, *67*(7), 468-471.

Holm, J., & Kleppa, O. (1966). The thermodynamic properties of the aluminum silicates. *American Mineralogist: Journal of Earth and Planetary Materials*, *51*(11-12), 1608-1622.

Hong, J. S., Huang, X. X., & Guo, J. K. (1995). Synthesis and sintered properties of mullite powder from seeded diphasic Al2O3-SiO2 gel. *Materials Letters*, *24*(5), 327-331. https://doi.org/https://doi.org/10.1016/0167-577X(95)00118-2

Hossain, S., Pyare, R., & Roy, P. (2020). Synthesis of in-situ mullite foam using waste rice husk ash derived sol by slip-casting route. *Ceramics International*, *46*(8), 10871-10878.

Hossain, S. S., Baek, I.-W., Son, H.-J., Park, S., & Bae, C.-J. (2022). 3D printing of porous low-temperature in-situ mullite ceramic using waste rice husk ash-derived silica. *Journal of the European Ceramic Society*, *42*(5), 2408-2419.

Hossain, S. S., Mathur, L., & Roy, P. (2018). Rice husk/rice husk ash as an alternative source of silica in ceramics: A review. *Journal of Asian Ceramic Societies*, *6*(4), 299-313.

Hu, M. Z.-C., Zielke, J., Byers, C., Lin, J., & Harris, M. (2000). Probing the early-stage/rapid processes in hydrolysis and condensation of metal alkoxides. *Journal of materials science*, *35*, 1957-1971.

Huling, J. C., & Messing, G. L. (1991). Epitactic nucleation of spinel in aluminosilicate gels and its effect on mullite crystallization. *Journal of the American Ceramic Society*, *74*(10), 2374-2381.

Hyung Mi, L., Jinho, L., Jeong-Hwan, J., Seong-Geun, O., & Seung-Ho, L. (2010). Comparative study of various preparation methods of colloidal silica. *Engineering*, *2010*.

Innocenzi, P. (2023). Sol-gel processing for advanced ceramics, a perspective. *Open Ceramics*, 100477.

JAGANNATH, R., NARAYAN, B., SANTANU, D., & SAIKAT, M. (2011). Studies on the formation of mullite from diphasic Al2O3-SiO2 gel by fourier transform infrared spectroscopy.

Jana, A., & Ray, D. (2020). Synthesis and characterization of sol-gel derived monophasic mullite powder. *Cerâmica*, *66*, 307-313.

Janackovic, D., Jokanovic, V., Kostic-Gvozdenovic, L., & Uskokovic, D. (1998). Synthesis of mullite nanostructured spherical powder by ultrasonic spray pyrolysis. *Nanostructured materials*, *10*(3), 341-348.

Janaćković, D., Jokanović, V., Kostić-Gvozdenović, L., Živković, L., & Uskoković, D. (1996). Synthesis, morphology, and formation mechanism of mullite particles produced by ultrasonic spray pyrolysis. *Journal of Materials Research*, *11*(7), 1706-1716.

Jaymes, I., Douy, A., Massiot, D., & Coutures, J. (1996). Characterization of mono-and diphasic mullite precursor powders prepared by aqueous routes. 27Al and 29Si MAS-NMR spectroscopy investigations. *Journal of materials science*, *31*(17), 4581-4589.

Johnson, B. R., Kriven, W. M., & Schneider, J. (2001). Crystal structure development during devitrification of quenched mullite. *Journal of the European Ceramic Society*, *21*(14), 2541-2562.

Kansal, P., Laine, R. M., & Babonneau, F. (1997). A processable mullite precursor prepared by reacting silica and aluminum hydroxide with triethanolamine in ethylene glycol: structural evolution on pyrolysis. *Journal of the American Ceramic Society*, *80*(10), 2597-2606.

Kara, F., & Little, J. (1996). Sintering behaviour of precursor mullite powders and resultant microstructures. *Journal of the European Ceramic Society*, *16*(6), 627-635.

Karhu, M., Lagerbom, J., Solismaa, S., Honkanen, M., Ismailov, A., Räisänen, M.-L., Huttunen-Saarivirta, E., Levänen, E., & Kivikytö-Reponen, P. (2019). Mining tailings as raw

materials for reaction-sintered aluminosilicate ceramics: Effect of mineralogical composition on microstructure and properties. *Ceramics International*, *45*(4), 4840-4848.

Keziz, A., Heraiz, M., Sahnoune, F., & Rasheed, M. (2023). Characterization and mechanisms of the phase's formation evolution in sol-gel derived mullite/cordierite composite. *Ceramics International*, *49*(20), 32989-33003.

Keziz, A., Rasheed, M., Heraiz, M., Sahnoune, F., & Latif, A. (2023). Structural, morphological, dielectric properties, impedance spectroscopy and electrical modulus of sintered Al6Si2O13–Mg2Al4Si5O18 composite for electronic applications. *Ceramics International*, *49*(23), 37423-37434.

Kim, J.-W., Lee, J.-E., Jung, Y.-G., Jo, C.-Y., Lee, J.-H., & Paik, U. (2003). Synthesis behavior and grain morphology in mullite ceramics with precursor pH and sintering temperature. *Journal of Materials Research*, *18*(1), 81-87.

Komarneni, S., & Rutiser, C. (1996). Single-phase and diphasic aerogels and xerogels of mullite: Preparation and characterization. *Journal of the European Ceramic Society*, *16*(2), 143-147. https://doi.org/https://doi.org/10.1016/0955-2219(95)00141-7

Kool, A., Thakur, P., Bagchi, B., Sepay, N., & Das, S. (2016). Physico-chemical property-driven dielectric behaviour and catalytic activity of nanocrystalline mullite synthesized from monophasic precursor gel. *Journal of Sol-Gel Science and Technology*, *80*, 769-782.

Krenzel, T. F., Schreuer, J., Laubner, D., Cichocki, M., & Schneider, H. (2019). Thermo-mechanical properties of mullite ceramics: New data. *Journal of the American Ceramic Society*, *102*(1), 416-426.

Lamara, S., Sahnoune, F., Saheb, N., Redaoui, D., & Laziri, K. (2022). Kinetics of mullitization from sol-gel synthesized precursors. *Journal of the Indian Chemical Society*, *99*(6), 100473.

Lee, J.-E., Kim, J.-W., Jung, Y.-G., Jo, C.-Y., & Paik, U. (2002). Effects of precursor pH and sintering temperature on synthesizing and morphology of sol–gel processed mullite. *Ceramics International*, *28*(8), 935-940.

Lee, J.-E., Kim, J.-W., Jung, Y.-G., & Paik, U. (2003). Effects of precursor pH and composition on the grain morphology and size of mullite ceramics in aqueous system. *Materials Letters*, *57*(21), 3239-3244.

Lee, J.-E., Kim, J.-W., Lee, J.-H., Jung, Y.-G., & Paik, U. (2004). Mullite precursor synthesis in aqueous conditions: dependence of mullite crystallization and grain size and morphology on solution pH and precursor salt. *Journal of Materials Research*, *19*, 1133-1138.

Lenz, S., Birkenstock, J., Fischer, L. A., Schneider, H., & Fischer, R. X. (2020). Mullite-2 c–a natural polytype of mullite. *European Journal of Mineralogy*, *32*(2), 235-249.

Li, D. X., & Thomson, W. J. (1990). Mullite formation kinetics of a single-phase gel. *Journal of the American Ceramic Society*, *73*(4), 964-969.

Li, D. X., & Thomson, W. J. (1991). Tetragonal to orthorhombic transformation during mullite formation. *Journal of Materials Research*, *6*(4), 819-824.

Lima, L., Silva, K., Menezes, R., Santana, L., & Lira, H. (2022). Microstructural characteristics, properties, synthesis and applications of mullite: a review. *Cerâmica*, *68*, 126-142.

Lima, L. K. S., Silva, K. R., Menezes, R. R., Santana, L. N. L., & Lira, H. L. (2022). Microstructural characteristics, properties, synthesis and applications of mullite: a review. *Cerâmica*, *68*.

Liu, D., Gui, K., Long, J., Zhao, Y., Han, W., & Wang, G. (2020). Low-temperature densification and mechanical properties of monolithic mullite ceramic. *Ceramics International*, *46*(8, Part B), 12329-12334. https://doi.org/https://doi.org/10.1016/j.ceramint.2020.01.282

Liu, Y., Lian, W., Su, W., Luo, J., & Wang, L. (2020). Synthesis and mechanical properties of mullite ceramics with coal gangue and wastes refractory as raw materials. *International Journal of Applied Ceramic Technology*, *17*(1), 205-210.

Ma, Q., Peng, H., Duan, L., & Chen, Z. (2014). Porous mullite ceramics fabricated by co-pyrolysis alumina powders filled silicone resin. *Materials Research Innovations*, *18*(sup4), S4-691-S694-694.

Mahnicka-Goremikina, L., Svinka, R., Svinka, V., Goremikins, V., Ilic, S., Grase, L., Juhnevica, I., Rundans, M., Eiduks, T. V., & Pludons, A. (2023). Porous Mullite Ceramic Modification with Nano-WO3. *Materials*, *16*(13), 4631. https://www.mdpi.com/1996-1944/16/13/4631

McLean, D. (1967). Dielectric Materials and Capacitor Miniaturization. *IEEE Transactions on Parts, Materials and Packaging*, *3*(4), 163-169. https://doi.org/10.1109/TPMP.1967.1135735

Miao, C., Liang, L., Zhang, F., Chen, S., Shang, K., Jiang, J., Zhang, Y., & Ouyang, J. (2022). Review of the fabrication and application of porous materials from silicon-rich industrial solid waste. *International Journal of Minerals, Metallurgy and Materials*, *29*(3), 424-438.

Milea, C., Bogatu, C., & Duta, A. (2011). The influence of parameters in silica sol-gel process. *Bulletin of the Transilvania University of Brasov. Series I-Engineering Sciences*, 59-66.

Mohammed, A. A., Khodair, Z. T., & Khadom, A. A. (2020). Preparation and investigation of the structural properties of α-Al2O3 nanoparticles using the sol-gel method. *Chemical Data Collections*, *29*. https://doi.org/10.1016/j.cdc.2020.100531

Mulpuri, R. P., & Sarin, V. K. (1996). Synthesis of mullite coatings by chemical vapor deposition. *Journal of Materials Research*, *11*(6), 1315-1324.

Nair, S. G., Sreejith, K., Jayalatha, C., & Prabhakaran, K. (2024). Mullite crystallization in zirconia incorporated aluminosilicate ceramics prepared from novel monophasic liquid precursor. *Ceramics International*, *50*(6), 8602-8613.

Nketia-Yawson, B., & Noh, Y. Y. (2018). Recent progress on high-capacitance polymer gate dielectrics for flexible low-voltage transistors. *Advanced Functional Materials*, *28*(42), 1802201.

Okada, K., & ŌTSUKA, N. (1986). Characterization of the spinel phase from SiO2-Al2O3 xerogels and the formation process of mullite. *Journal of the American Ceramic Society*, *69*(9), 652-656.

Oliveira, F. C., Livramento, V., & Delmas, F. (2008). Novel mullite-based ceramics manufactured from inorganic wastes: I. Densification behaviour. *Journal of Materials Processing Technology*, *196*(1-3), 101-108.

Otitoju, T. A., Okoye, P. U., Chen, G., Li, Y., Okoye, M. O., & Li, S. (2020). Advanced ceramic components: Materials, fabrication, and applications. *Journal of industrial and engineering chemistry*, *85*, 34-65.

Pa, F. C., Chik, A., Bari, M. F., & Noorina, H. J. (2014). Extraction of silica from palm ash using organic acid leaching treatment. *Key Engineering Materials*, *594*, 329-333.

Padmaja, P., Anilkumar, G., Mukundan, P., Aruldhas, G., & Warrier, K. (2001). Characterisation of stoichiometric sol–gel mullite by fourier transform infrared spectroscopy. *International Journal of Inorganic Materials*, *3*(7), 693-698.

Padmaja, P., Anilkumar, G. M., Mukundan, P., Aruldhas, G., & Warrier, K. G. K. (2001). Characterisation of stoichiometric sol–gel mullite by fourier transform infrared spectroscopy. *International Journal of Inorganic Materials*, *3*(7), 693-698. https://doi.org/https://doi.org/10.1016/S1466-6049(01)00189-1

Pani, S., Kumar Sahoo, R., Dash, N., Kumar Singh, S., & Kumar Mohapatra, B. (2015). Cost effective and minimal time synthesis of mullite from a mine waste by thermal plasma process. *Advanced Materials Letters*, *6*(4), 318-323.

Parashar, M., Shukla, V. K., & Singh, R. (2020). Metal oxides nanoparticles via sol–gel method: a review on synthesis, characterization and applications. *Journal of Materials Science: Materials in Electronics*, *31*(5), 3729-3749.

Park, J. Y., Gu, Y. M., Park, S. Y., Hwang, E. T., Sang, B.-I., Chun, J., & Lee, J. H. (2021). Two-Stage Continuous Process for the Extraction of Silica from Rice Husk Using Attrition Ball Milling and Alkaline Leaching Methods. *Sustainability*, *13*(13), 7350. https://www.mdpi.com/2071-1050/13/13/7350

Pask, J. A., Zhang, X., Tomsia, A., & Yoldas, B. (1987). Effect of Sol-Gel Mixing on Mullite Microstructure and Phase Equilibria in the α-Al2O3-SiO2 System. *Journal of the American Ceramic Society*, *70*(10), 704-707.

Pattipaka, S., Lim, Y., Son, Y. H., Bae, Y. M., Peddigari, M., & Hwang, G.-T. (2024). Ceramic-Based Dielectric Materials for Energy Storage Capacitor Applications. *Materials*, *17*(10), 2277. https://www.mdpi.com/1996-1944/17/10/2277

Razak, N. A. A., Othman, N. H., Shayuti, M. S. M., Jumahat, A., Sapiai, N., & Lau, W. J. (2022). Agricultural and industrial waste-derived mesoporous silica nanoparticles: A review on chemical synthesis route. *Journal of Environmental Chemical Engineering*, *10*(2), 107322.

Rödel, J., Kounga, A. B., Weissenberger-Eibl, M., Koch, D., Bierwisch, A., Rossner, W., Hoffmann, M. J., Danzer, R., & Schneider, G. (2009). Development of a roadmap for advanced ceramics: 2010–2025. *Journal of the European Ceramic Society*, *29*(9), 1549-1560.

Romero, M., Padilla, I., Contreras, M., & López-Delgado, A. (2021). Mullite-Based Ceramics from Mining Waste: A Review. *Minerals*, *11*(3), 332. https://www.mdpi.com/2075-163X/11/3/332

Roy, J., Das, S., & Maitra, S. (2015). Solgel-processed mullite coating—a review. *International Journal of Applied Ceramic Technology*, *12*, E71-E77.

Roy, J., & Maitra, S. (2014). Synthesis and characterization of sol-gel-derived chemical mullite. *J. Ceram. Sci. Tech*, *5*, 57-62.

Roy, R., Das, D., & Rout, P. K. (2021). A review of advanced mullite ceramics. *Engineered Science*, *18*, 20-30.

Sadanaga, R., Tokonami, M., & Takeuchi, Y. (1962). The structure of mullite, 2Al2O3. SiO2, and relationship with the structures of sillimanite and andalusite. *Acta Crystallographica*, *15*(1), 65-68.

Sahnoune, F., Chegaar, M., Saheb, N., Goeuriot, P., & Valdivieso, F. (2008). Differential thermal analysis of mullite formation from Algerian kaolin. *Advances in applied ceramics*, *107*(1), 9-13.

Sales, M., & Alarcón, J. (1996). Synthesis and phase transformations of mullites obtained from SiO2□ Al2O3 gels. *Journal of the European Ceramic Society*, *16*(7), 781-789.

Sánchez-Ramírez, E., Ramírez-Márquez, C. s., Quiroz-Ramírez, J. J., Contreras-Zarazúa, G., Segovia-Hernández, J. G., & Cervantes-Jauregui, J. A. (2018). Reactive distillation column design for tetraethoxysilane (TEOS) production: economic and environmental aspects. *Industrial & Engineering Chemistry Research*, *57*(14), 5024-5034.

Sánchez-Soto, P. J., Eliche-Quesada, D., Martínez-Martínez, S., Garzón-Garzón, E., Pérez-Villarejo, L., & Rincón, J. M. (2018). The effect of vitreous phase on mullite and mullite-based ceramic composites from kaolin wastes as by-products of mining, sericite clays and kaolinite. *Materials Letters*, *223*, 154-158.

Sánchez-Soto, P. J., Eliche-Quesada, D., Martínez-Martínez, S., Pérez-Villarejo, L., & Garzón, E. (2022). Study of a waste kaolin as raw material for mullite ceramics and mullite refractories by reaction sintering. *Materials*, *15*(2), 583.

Schmidt, H. (1985). New type of non-crystalline solids between inorganic and organic materials. *Journal of Non-Crystalline Solids*, *73*(1-3), 681-691.

Schmidt, H., & Scholze, H. (1985). Mechanisms and kinetics of the hydrolysis and condensation of alkoxides. In *Glass… Current Issues* (pp. 263-280). Springer.

Schmidt, H., Scholze, H., & Kaiser, A. (1984). Principles of hydrolysis and condensation reaction of alkoxysilanes. *Journal of Non-Crystalline Solids*, *63*(1-2), 1-11.

Schmidt, J., Altun, A. A., Schwentenwein, M., & Colombo, P. (2019). Complex mullite structures fabricated via digital light processing of a preceramic polysiloxane with active alumina fillers. *Journal of the European Ceramic Society*, *39*(4), 1336-1343. https://doi.org/10.1016/j.jeurceramsoc.2018.11.038

Schneider, H., Fischer, R. X., & Schreuer, J. (2015). Mullite: crystal structure and related properties. *Journal of the American Ceramic Society*, *98*(10), 2948-2967.

Schneider, H., & Komarneni, S. (2006). *Mullite*. John Wiley & Sons.

Schneider, H., Schreuer, J., & Hildmann, B. (2008). Structure and properties of mullite—A review. *Journal of the European Ceramic Society*, *28*(2), 329-344.

Sembiring, S., Simanjuntak, W., Manurung, P., Asmi, D., & Low, I. M. (2014). Synthesis and characterisation of gel-derived mullite precursors from rice husk silica. *Ceramics International*, *40*(5), 7067-7072.

Song, F. S. (2011). Needle-like mullite ceramic prepared by sol-gel process. *Advanced Materials Research*, *233*, 2640-2643.

Tan, H., Ding, Y., & Yang, J. (2010). Mullite fibres preparation by aqueous sol–gel process and activation energy of mullitization. *Journal of alloys and compounds*, *492*(1-2), 396-401.

Tejaswini, M. S. S. R., Pathak, P., & Gupta, D. K. (2022). Sustainable approach for valorization of solid wastes as a secondary resource through urban mining. *Journal of Environmental Management*, *319*, 115727. https://doi.org/https://doi.org/10.1016/j.jenvman.2022.115727

Tesfaye, R. M., Teklemariam, F., Aweke, H., & Gebregwergis, H. (2022). Synthesis and characterization of silica from awash melkaasa chemical factory waste. *Ethiopian Journal of Science and Sustainable Development*, *9*(2), 62-67.

Tessema, B., Gonfa, G., Mekuria Hailegiorgis, S., & Venkatesa Prabhu, S. (2023). An overview of current and prognostic trends on synthesis, characterization, and applications of biobased silica. *Advances in Materials Science and Engineering*, *2023*.

Tiffo, E., Elimbi, A., Manga, J. D., & Tchamba, A. B. (2015a). Red ceramics produced from mixtures of kaolinite clay and waste glass. *Brazilian Journal of Science and Technology*, *2*, 1-13.

Tiffo, E., Elimbi, A., Manga, J. D., & Tchamba, A. B. (2015b). Red ceramics produced from mixtures of kaolinite clay and waste glass. *Brazilian Journal of Science and Technology*, *2*(1), 4. https://doi.org/10.1186/s40552-015-0009-9

USHIFUSA, N., SAKAMOTO, K., NAGAYAMA, K., & OGIHARA, S. (1990). Study of Mullite-Glass Ceramics for Substrates. *Journal of the Ceramic Society of Japan*, *98*(1136), 377-383.

Ushifusa, N., Sakamoto, K., Ogihara, S., & Fujita, T. (1992). Properties and Microstructure of Mullite-Glass Ceramics for Multilayer Ceramic Substrates. *MRS Online Proceedings Library*, *264*(1), 31-36. https://doi.org/10.1557/PROC-264-31

Vaibhav, V., Vijayalakshmi, U., & Roopan, S. M. (2015). Agricultural waste as a source for the production of silica nanoparticles. *Spectrochimica acta part A: Molecular and biomolecular spectroscopy*, *139*, 515-520.

Vieira, M., Catarino, L., Oliveira, M., Sousa, J., Torralba, J., Cambronero, L., González-Mesones, F., & Victoria, A. (1999). Optimization of the sintering process of raw material wastes. *Journal of Materials Processing Technology*, *92*, 97-101.

Vieira, S., Ramos, A., & Vieira, M. (2007). Mullitization kinetics from silica-and alumina-rich wastes. *Ceramics International*, *33*(1), 59-66.

Vinai, R., & Soutsos, M. (2019). Production of sodium silicate powder from waste glass cullet for alkali activation of alternative binders. *Cement and Concrete Research*, *116*, 45-56.

Wahab, R. A. A., Yahya, M. A., Matori, K. A., & Ghani, W. A. W. A. K. (2017). Effects of Sintering Temperature on the Mullite-Based Ceramics Fabricated from Rice Husk Ash. *Applied Mechanics and Materials*, *873*, 65-70.

Wang, X., Sun, H., Wang, M., Tang, M., Lan, Y., Xu, R., Feng, Y., Li, Z., Wei, X., & Xu, Z. (2024). Low-temperature sintering of PLSZT-based antiferroelectric ceramics in reducing atmosphere for energy storage. *Journal of the European Ceramic Society*, *44*(2), 898-906. https://doi.org/https://doi.org/10.1016/j.jeurceramsoc.2023.09.053

WEI, W. C., & Halloran, J. W. (1988a). Phase transformation of diphasic aluminosilicate gels. *Journal of the American Ceramic Society*, *71*(3), 166-172.

WEI, W. C., & Halloran, J. W. (1988b). Transformation kinetics of diphasic aluminosilicate gels. *Journal of the American Ceramic Society*, *71*(7), 581-587.

Won, C.-W., & Siffert, B. (1998a). Preparation by sol-gel method of SiO2 and mullite (3Al2O3, 2SiO2) powders and study of their surface characteristics by inverse gas chromatography and zetametry. *Colloids and Surfaces A: Physicochemical and Engineering Aspects*, *131*(1), 161-172. https://doi.org/https://doi.org/10.1016/S0927-7757(97)00149-0

Won, C.-W., & Siffert, B. (1998b). Preparation by sol-gel method of SiO2 and mullite (3Al2O3, 2SiO2) powders and study of their surface characteristics by inverse gas chromatography and zetametry. *Colloids and Surfaces A: Physicochemical and Engineering Aspects*, *131*(1-3), 161-172.

Worrall, D. (1986). *Clays and ceramic raw materials*. Springer Science & Business Media.

Xia, B., Wang, Z., Gou, L., Zhang, M., & Guo, M. (2022). Porous mullite ceramics with enhanced compressive strength from fly ash-based ceramic microspheres: Facile synthesis, structure, and performance. *Ceramics International*, *48*(8), 10472-10479. https://doi.org/https://doi.org/10.1016/j.ceramint.2021.12.256

Xu, X., Liu, X., Wu, J., Zhang, C., Zhou, S., & Wu, C. (2021). Fabrication and characterization of porous mullite ceramics with ultra-low shrinkage and high porosity via sol-gel and solid state reaction methods. *Ceramics International*, *47*(14), 20141-20150. https://doi.org/https://doi.org/10.1016/j.ceramint.2021.04.020

Yan, Z., Gao, Y., & Zhang, H. (2023). Materials Development and Potential Applications of Ceramics: New Opportunities and Challenges. *Applied Sciences*, *13*(19), 10957. https://www.mdpi.com/2076-3417/13/19/10957

Yin, Q., Zhu, B., & Zeng, H. (2010). Review and prospect of functional ceramics. *Microstructure, Property and Processing of Functional Ceramics*, 337-363.

Yu, H., Zahidi, I., Fai, C. M., Liang, D., & Madsen, D. Ø. (2024). Mineral waste recycling, sustainable chemical engineering, and circular economy. *Results in Engineering*, *21*, 101865. https://doi.org/https://doi.org/10.1016/j.rineng.2024.101865

Yugeswaran, S., Selvarajan, V., Lusvarghi, L., Karoly, Z., & Szepvolgyi, J. (2011). Synthesis of mullite from laboratory waste silica through transferred arc plasma processing method. *Materials and Manufacturing Processes*, *26*(6), 813-820.

Yuvakkumar, R., Elango, V., Rajendran, V., & Kannan, N. (2014). High-purity nano silica powder from rice husk using a simple chemical method. *Journal of experimental nanoscience*, *9*(3), 272-281.

Zhai, K., Xue, W., Wang, H., Wu, X., & Zhai, S. (2020). Raman spectra of sillimanite, andalusite, and kyanite at various temperatures. *Physics and Chemistry of Minerals*, *47*(5), 23. https://doi.org/10.1007/s00269-020-01092-9

Zhang, B., Ma, J., Ye, J., Jin, Y., Yang, C., Ding, J., Zhang, Z., Hou, Z., Liu, Q., & Ye, F. (2019). Ultra-low cost porous mullite ceramics with excellent dielectric properties and low thermal conductivity fabricated from kaolin for radome applications. *Ceramics International*, *45*(15), 18865-18870. https://doi.org/https://doi.org/10.1016/j.ceramint.2019.06.120

Zhang, T., Du, J., Lei, Y., Cheng, Y., Liu, W., Yi, X., Yin, J., & Yu, P. (2020). Effect of pores on dielectric breakdown strength of alumina ceramics via surface and volume effects. *Journal of the European Ceramic Society*, *40*(8), 3019-3026.

Zhang, T., Lei, Y., Yin, J., Du, J., & Yu, P. (2019). Effects of pores on dielectric breakdown of alumina ceramics under AC electric field. *Ceramics International*, *45*(11), 13951-13957. https://doi.org/https://doi.org/10.1016/j.ceramint.2019.04.093

Zhang, Y., Ding, Y., Gao, J., & Yang, J. (2009). Mullite fibres prepared by sol–gel method using polyvinyl butyral. *Journal of the European Ceramic Society*, *29*(6), 1101-1107. https://doi.org/https://doi.org/10.1016/j.jeurceramsoc.2008.08.008

Zhao, H., Hiragushi, K., & Mizota, Y. (2002). Phase segregation of non-stoichiometric aluminosilicate gels characterized by 27Al and 29Si MAS-NMR. *Journal of Non-Crystalline Solids*, *311*(2), 199-206. https://doi.org/https://doi.org/10.1016/S0022-3093(02)01635-6

Appendix A

PDF Card of Mullite

PDF Card

PDF Number	00-015-0776	**Status**	Primary	**Quality Mark**		Indexed
Pressure/Temperature	Ambient					
Chemical Formula	Al6 Si2 O13					
Structural Formula						
Empirical Formula	Al6 O13 Si2					
Weight %	Al38.00 O48.82 Si13.18					
Atomic %	Al28.57 O61.90 Si9.52					
Compound Name	Aluminum Silicate					
ANX						
Mineral Name	Mullite, syn					
Also Called						

Experimental	**Rad**	λ	**Filter**	**d-Spacing**	**Cutoff**	**Intensity**	**I/Ic**
	CuKα	1.5406	Ni Beta			Diffractometer	
	Camera Diameter						

	SYS	**Space Group**	**Aspect**	**Cell Wave Vector 1**	**Cell Wave Vector 2**
	Orthorhombic	Pbam (55)			

Physical	**Subsystems**	ID W Matrix					
	Author's Cell	**a**	**b**	**c**	α	β	γ
		7.5456	7.6898	2.8842			
		Volume	**Z**	**Molecular Volume/Formula Unit Volume**			
		167.35	0.75	223.13			
	Author's Cell Axial Ratio	**c/a**	**a/b**	**c/b**			
		0.382	0.981	0.375			
	Density	**Dcalc**	**Dmeas**	**Dstruc**			
		3.171	3				
	SS/FOM	**Temperature**	**Melting Point**	**R-factor**	**Error**		
	F(30) = 60.4 (0.0134, 37)	298.000					

	Space Group	**Molecular Weight**					
	Pbam (55)	426.05					
	Crystal Data	**a**	**b**	**c**	α	β	γ
		7.546	7.690	2.884	90.00	90.00	90.00
		Volume	**Z**				

Appendix B

The formation of soda silicate glass from silica extraction residue

In silica extraction process, after basic treatment there are residue which is by product of sodium silicate solution. So, in this residue I perform some progress to characterize and unlock what importance might it have. After XRD and TGA characterization, it revealed that this residue has the capacity to form soda silicate glasses. And one of major advantage of it has less melting point about 1200 C. for further clarification here has been presented some data. XRD data also showed the formation of soda silicate glass which is similar with other worked research (Tiffo et al., 2015a).

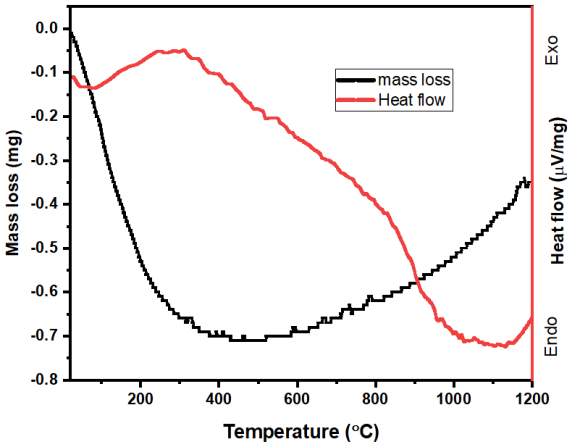

Figure A. 1: Shows TGA/DTA graph of silica extraction residue

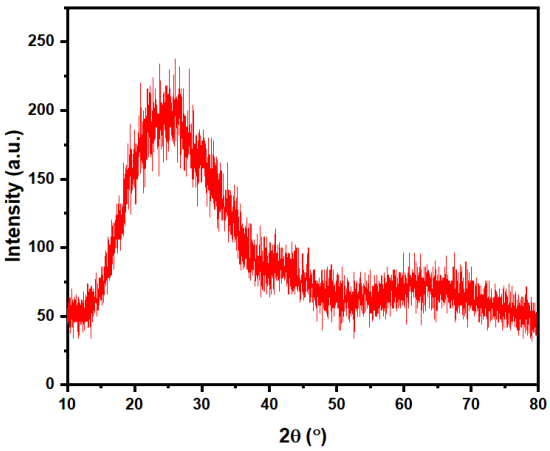

Figure A. 2: XRD pattern of silica extraction residue after 1250 ^{0}C firing

Appendix C

Visual Documentation

Figure C.1: Visual documentation of a) Water bath b) Electronic balance c) Digital verner caliper d) Compression strength testing machine e) Dielectric strength testing machine